View metadata, citation and similar papers at core.ac.uk

brought to you by CORE

provided by Digital Repository @ Iowa State University

IOWA STATE UNIVERSITY
Digital Repository

Retrospective Theses and Dissertations

Iowa State University Capstones, Theses and Dissertations

1-1-2000

Amorphous silicon carbide solar cells fabricated using ECR-PECVD

Vu Anh Vu
Iowa State University

Follow this and additional works at: https://lib.dr.iastate.edu/rtd

 Part of the Electrical and Computer Engineering Commons

Recommended Citation

Vu, Vu Anh, "Amorphous silicon carbide solar cells fabricated using ECR-PECVD" (2000). *Retrospective Theses and Dissertations*. 17812.
https://lib.dr.iastate.edu/rtd/17812

This Thesis is brought to you for free and open access by the Iowa State University Capstones, Theses and Dissertations at Iowa State University Digital Repository. It has been accepted for inclusion in Retrospective Theses and Dissertations by an authorized administrator of Iowa State University Digital Repository. For more information, please contact digirep@iastate.edu.

Amorphous silicon carbide solar cells fabricated using ECR-PECVD

by

Vu Anh Vu

A thesis submitted to the graduate faculty
In partial fulfillment of the requirements for the degree of
MASTER OF SCIENCE

Major: Electrical Engineering
Major Professor: Vikram L. Dalal

Iowa State University
Ames, Iowa
2000

Graduate College

Iowa State University

This is to certify that the Master's thesis of

Vu Anh Vu

has meet the thesis requirements of Iowa State University

Signatures have been redacted for privacy

TABLE OF CONTENTS

ABSTRACT

Solar power is becoming important as an alternative energy source. Solar power generation utilizes solar cells, which generates DC electricity when light falls on them. Attractive materials for solar energy conversion are amorphous silicon (a-Si) and its alloys, such as amorphous silicon carbide (a-(SiC)). Although research on a-Si solar cells has been carried out in many countries since the 1970's, a-(SiC) solar cells have not been widely studied. Amorphous silicon carbide has a wider bandgap than amorphous silicon; therefore, we can expect to have solar cells with larger open-circuit voltage and high conversion efficiency for the high-energy spectrum in tandem-cell arrangement. High bandgap combined with good material quality leads to an increase in open-circuit voltage. The work presented here explores the relationship between photovoltaic properties and growth conditions of amorphous silicon carbide solar cells. With this, we are able to determine a good fabrication technique for making a-SiC:H solar cells.

In this thesis, we study film quality by measuring Urbach energy, E_{04} and Tauc gaps, photo and dark conductivities, mobility-lifetime product, and activation energy. This report also studies the variation of these properties as functions of the growth conditions, such as substrate temperature, microwave power, chamber pressure, gas ratios, and doping levels. Then we applied the best growth conditions for making intrinsic and doped amorphous silicon carbide materials to produce good p-i-n solar cells.

We found that a deposition pressure of 10 mTorr, a substrate temperatures of 300 to 350^0C, and $CH_4/(CH_4+SiH_4)$ flows of 0.6 to 0.7 can produce very good amorphous silicon carbide solar cells. These solar cells have an open-circuit voltage of 0.96 V, and a fill factor of 0.71. We also found that our materials have superior quality compared to materials reported previously in the literature.

CHAPTER 1: INTRODUCTION

1.1 Purpose of research

Amorphous silicon solar cell technology has evolved considerably since the first amorphous silicon solar cells were made at RCA Laboratories in 1974. Scientists working in a number of laboratories worldwide have been able to improve alloys based on hydrogenated amorphous silicon and microcrystalline silicon.

The conversion efficiency of solar cells is high when the photon energy is in the range of its bandgap. Therefore, solar cells manufactured from a single semiconductor material cannot have high conversion efficiency. If we consider dividing the solar radiation spectrum into different wavelength ranges, we can then use a different semiconducting material for each range. For example, if a-SiC:H is used for the high energy range (short wavelength), a-Si:H is used for the middle energy range, and a-SiGe:H is used for the low energy range, then the conversion efficiency can be improved significantly.

Although a-SiC:H has been used as a window material for a-Si:H solar cells to increase fill factor, a-SiC:H solar cells (a-SiC:H in the i-layer) have not been widely developed. The p-layer itself is believed to be a dead layer (layer in which the excited carriers do not contribute to the photo current), and the collection efficiency improves when a-SiC:H is used for the p-layer since the amount of absorption in the p-layer decreases due to the increase of the forbidden bandgap. Since the i-layer is an active layer, it should meet a certain standard requirement for making a solar cell. Amorphous silicon carbide generally has a higher defect density than amorphous silicon; therefore, we need to research the growth conditions to make good solar cells.

In this thesis, we will report on the effects of growth conditions on the optical and electrical properties of amorphous silicon carbide thin films prepared by ECR-PECVD from a mixture of silane (SiH_4), methane (CH_4), and hydrogen (H_2). We will also investigate the effects of boron and phosphorus doping by using diborane (B_2H_6) and phosphine (PH_3) as the doping gases. Then we will apply the best growth conditions for making intrinsic and doped amorphous silicon carbide to make p-i-n solar cells.

1.2 Fundamental of amorphous semiconductors

Amorphous materials are characterized by a lack of any periodic arrangement of atoms. Unlike amorphous metals, amorphous semiconductors do not consist of close-packed atoms, but rather they contain covalently bonded atoms arranged in an open network with correlations in ordering up to the third or fourth nearest neighbors. The short range order is directly responsible for observable semiconductor properties such as optical absorption edges and activated electrical conductivities [1]. A system with an indirect bandgap in the crystalline state becomes a direct bandgap in the amorphous state. The conduction and valence bands creating this bandgap contain extended states allowing free electron and hole travel.

In the present of hydrogen, the quality of amorphous semiconductor meets the general requirement for electronic and optical application. What hydrogen does is to find the unbounded Si bonds in the network and attach them to make the local charge neutral. When the hydrogen content in the network reaches about 10% atomic weight, the midgap defect states are in order of $10^{15}cm^{-3}eV^{-1}$. This gives reasonably good carrier transportation properties such as the carrier lifetime and mobility. When the DOS is larger than $10^{21}cm^{-3}eV^{-1}$, it is called extended states in which carriers behave like crystal. The states follow the extended states are called tail states. They are usually expressed as an exponential function of energy. The slope of this exponential function is called Urbach energy. The states follow the tail states are called midgap states. It should be about $10^{15}cm^{-3}eV^{-1}$ for a good amorphous material.

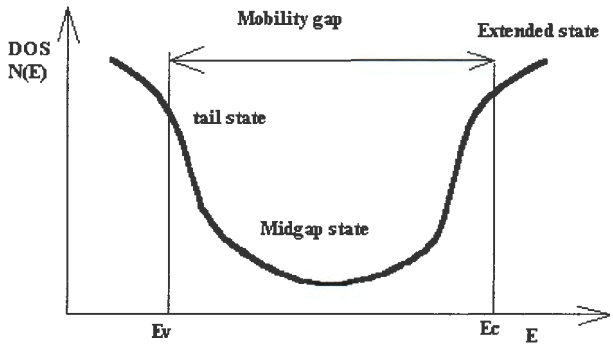

Figure 1.1: Density of states of amorphous semiconductor

1.3 Amorphous silicon carbide

Amorphous SiC is produced by incorporating carbon atoms (from methane) into the silicon structure during the growth process. The already disordered structure of amorphous Si becomes more disordered due to the addition of carbon atoms. This results in changing the material bandgap and opto-electronic properties.

A-SiC:H alloy is an important material for potential application in bipolar transistors, image sensors, photoreceptors, light-emitting diodes, photodiodes, and photovoltaic cells. The incorporation of carbon in a in a-Si:H matrix causes the reduction of photoelectronic quality, the increase of Urbach energy, and , hence, of the microstructural disorder[18]. From the structure point of view, four different phases have been identified in the graphitic C bondings in the alloy. They are considered the principal cause for the degradation and can be minimized by hydrogen bonded to carbon via CH_n (n = 2, 3) formation[5]. As for the stability aspects, these alloys are unstable under prolonged light irradiation and can undergo two types of photoinduced changes: photobleaching and photodarkering, which become more pronounced at a high carbon contents [5].

Amorphous silicon carbide has proved useful as a wide bandgap material in microelectronic devices. Although alloying carbon into amorphous hydrogenated silicon increases the optical bandgap, it also deteriorates the optoelectronic properties. Most significant is the decrease in photoconductivity and the increase the paramagnetic defect density with increased carbon content. A study confirmed that the Si-H stretching mode used to amount of microstructure consists of two independent absorptions corresponding to Si-H in the bulk and on the inner surface of microvoids [7]. Taken together, the reported work showed that increasing the carbon content increased the fraction of microvoids in a-SiC[3].

Successful attempts to improve the a-SiC film properties have been reported, such as H_2 dilution effect[10], deposition of μc-SiC with the remote plasma-enhanced chemical vapor deposition method[5], and growth of fluorinated alloys from SiF_4-C_2F_6-H_2 mixture[5]. Tetramethylsilane and tetramethyldisilane have also been used as alternative

feed [8]. In their case the incorporation of CH_3 groups have been observed, giving less connective network and microvoids.

1.4 Amorphous silicon carbide solar cells

Amorphous silicon carbide has a wide bandgap; therefore, the dark current is low and the open circuit voltage is high. Also, as the amount of transmitted light increases with larger forbidden bandgap, the short-circuit current decreases. The fill factor of amorphous solar cells is normally 0.6-0.7[13]. The fill factor is influenced by various parameters such as the resistive component and diode factor but, primarily, the reduction in fill factor of amorphous solar cells originates in the bias dependency of the photocurrent. The minority carrier diffusion length of amorphous solar cells is short; therefore, the photocurrent contribution from outside the electric field region is slight. Thus, with forward bias, the electric field strength within the i-layer is reduced and, as the depletion layer width narrows, photo current decreases (Figure 1.2).

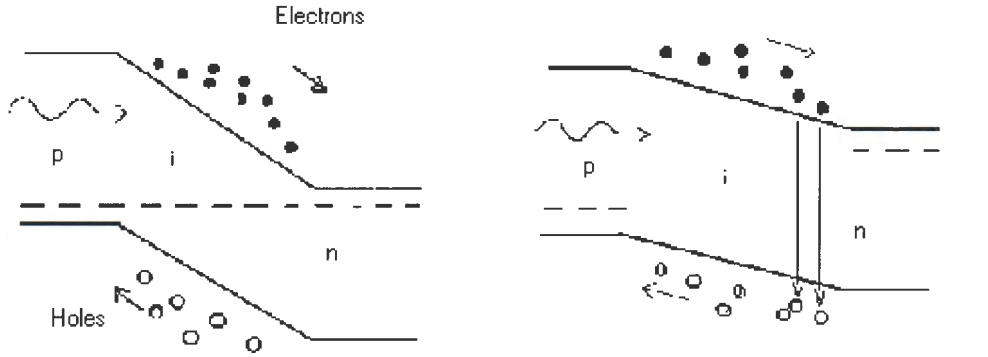

Figure 1.2 Band diagram of short and open circuit states

Also, the fill factor of amorphous solar cells is strongly dependent upon the incident light spectrum. When monochromatic light illuminates a p-i-n solar cells in which a strong electric field region exists at the p/i interface, the fill factor is large for the short wavelength light and small for long wavelength light. This is because the

absorption coefficient of amorphous SiC is small for long wavelength light so such light penetrates deep into the cell, with the result that the electron-hole pairs are generated some distance away from the junction region.

Amorphous p-n junctions do not usually display rectification properties, but display a more or less ohmic contact characteristic. There are many defect levels in p-layer and n-layer and as, carrier density is also high, the tunnel effect current becomes dominant. Therefore, a p-i-n type with an undoped layer between p-layer and n-layer is used in solar cells. As the density of i-layer defect levels is of the order of 10^{15} to 10^{16} $eV^{-1}cm^{-3}$, almost all the i-layer region forms a depletion layer and the generation of tunnel current is suppressed. In the amorphous solar cell, it is the i-layer that performs the photoelectric conversion, and the p-layer and n-layer are regarded as "dead" layers.

The most important properties of the materials used for p-layer are conductivity, thickness, and forbidden bandgap. The open-circuit voltage drops as the p-layer get thinner because the entire p-layer becomes a depletion layer, and so sufficient diffusion potential cannot be obtained. Conversely, as the p-layer becomes thicker, light absorption increases. When illuminated from the p-side, p-type amorphous silicon carbide with forbidden bandgap of approximately 2.0 eV is effective for use as a window layer. With a thin layer, the short wavelength light is transmitted to the i-layer so that both the short circuit current and the fill factor increase.

The optimum thickness for the i-layer depends upon localized state density. The thicker the i-layer, the more light is absorbed, but conversely, electric field decreases within the i-layer. This not only reduces the fill factor because of series resistance, but can also reduce the collection efficiency for the carriers excited near the i/n^+ interface. If the i-layer is thin, the fill factor increases due to the existence of a strong electric field across the entire i-layer region. Conversely, however, short-circuit current decrease because light absorption falls. According to our experiments, the i-layer thickness of 0.2 μm is the best choice.

Microcrystalline-n type Silicon carbide is a good choice for n- layer because the conductivity of μc layer is high and contact resistance with the metal layer drops. Furthermore, the optical bandgap of the μc layer is higher than that of i-layer; it allows

for efficient reflection of photons back into the i-layer. In this report, we have not worked on microcrystalline n- or p-(SiC) layers. We use rather a thin n^+ a-Si or a-(SiC) layer as a back up contact.

A microcrystalline (μc) is coated on top of the amorphous p-layer. Crystalline Si is an indirect transition material, so its coefficient of absorption is low. When the microcrystalline phase is mixed with the amorphous phase, the absorption coefficient is decreased. The number of photons reaching the i-layer is therefore increased, because of the reduced absorption loss in the p-layer. Finally, another amorphous p-layer is coated on the top of μc layer to prevent oxidation of the μc p-Si layer.

The bandgap of the i-layer is graded in the buffer layer at i/p interface so that its bandgap at the i-p interface is close to the bandgap of the p-layer (Figure 1.3). By doing that, the electric field is created to assist electrons though the interface and the quality of devices can be improved.

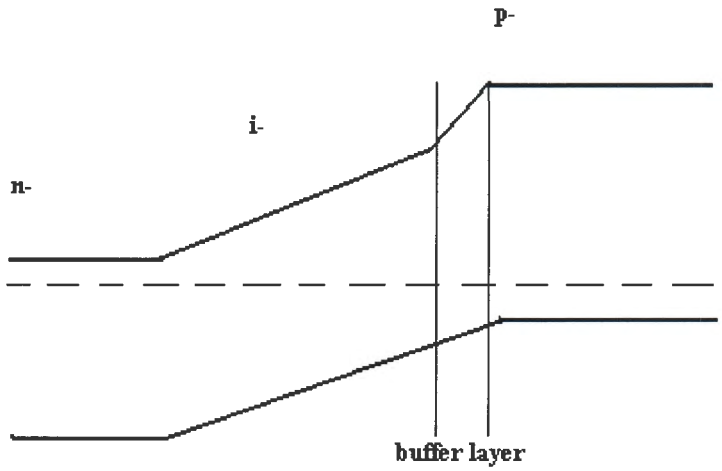

Figure 1.3 Band diagram of a solar cells with buffer layer

1.5 Fundamental of plasma

Plasma can be simply defined as partially ionized, quasineutral gas. If the very low number of charged particles (ions and electrons) existing in any gas at any temperature is increased by an external source, the electric field due to charge separation can become strong enough to limit particles' own motion and maintain the macroscopic neutrality; in that case ionized gas is called plasma. As there is a balance between the densities of negative and positive charges in macroscopic volumes and times, the more appropriate term quasineutrality is frequently used.

Among the various kinds of energy that can be applied, the electrical discharge is a simplest and widespread means to sustain plasma for a long time. Plasmas can be grouped into two generic categories: nonequilibrium and equilibrium. Under conditions of high electrical field applied for nonequilibrium plasmas generated at reduced pressure, free electrons are accelerated to high energies (1-10eV). However, because of their large mass, neutrals and ions in plasma have low energy. This energy difference results in a high temperature for the electrons, and a low or cool temperature of the neutrals and ions. Under these nonequilibrium conditions, the initiation of chemical reactions ocurs by collisions with the hot electrons. This allows the processing temperature to be much lower than in conventional thermal processes using similar chemistry. On the contrary, in thermal plasma all species have the same temperature, due to the shorter mean free path of particles and higher collision frequency characterizing higher-pressure condition. The application of an electric field is just a convenient way to supply the energy necessary to achieve a high temperature.

Over the last two decades, a large number of practical applications have been developed the field of nonequilibrium, or "cold" plasma science. Many new materials have becomes available with unique chemical, structural, and physical properties, which otherwise would not have been possible. As mentioned above, plasma processing allows the opportunity to synthesize materials a low temperature, while simultaneously allowing chemistry to result from dissociation or ionization of feed gas, which would have normally occurred in the thermal processes operated at much higher temperature.

1.6 Effects of gas dilution

The study on dilution has been carried out with the use of both noble gases and hydrogen. The dilution implies a depleting condition of the silane and methane flow rate and hence the deposition rate is limited. In the last few years, the gas dilution parameter has attracted considerable attention, because of its role in controlling the ion distribution in the gas phase, in material microstructure, and all the parameters affecting the material stability. A parameter related to the microstructure is usually utilized as quality probe of the material and defined by R as the fractional amount of SiH_2 groups to the total SiH_2 + SiH density; this is obtained by infrared absorption measurements of the relative stretching mode. As the SiH_2 configuration is associated mainly with the presence of microvoids in the sample, the R parameter is assumed to be correlated to the network microstructure and the material quality improves with decreasing R[14].

The CH_3 radicals abstract the H from the surface during the growth of the film and the appearance of H-deficient sites prevents the surface diffusion of SiH_3 radicals from finding their energetically favorable sites. In order to control the surface-H-coverage condition in the presence of CH_3 radicals, a sufficient amount of H atoms should be supplied from the gas phase, called hydrogen-dilution method. The effect of hydrogen dilution of silane and methane discharge has been studied from theoretical and experimental viewpoint.

Capotelli have found, through a theoretical calculation solving the Boltzmann equation, an increase of average electron energy with H_2 addition to SiH_4 plasma [12]. The collision frequencies for vibrational electronic excitation and ionization have been reported. The most important result is that in pure SiH_4 plasma the vibrational impact is 100 times more efficient than the electronic one, whereas in SiH_4-H_2 diluted plasmas the electronic excitation frequency become compatible to that of vibrational excitation.

From the experimental viewpoint, besides a pronounced variation in the plasma phase, strong changes have been found in the film properties. As an example, the amorphous-to-microcrystalline silicon transition is favored in Hydrogen highly diluted SiH_4 discharge at high power density or in sequential alternative discharges of SiH_4 and

H_2 gases; in this the H-atom density in plasma phase is very high and hence the interaction with the surface is strongly enhanced[15].

The chemical annealing preparation technique is also used for producing high quality amorphous silicon carbide films with a more stable network. The reactor used in chemical annealing technique is composed of a RF diode for decomposition of silane and methane, and a microwave plasma for the generation of H atoms and excited states of rare gases such as helium. Although the material contains very low H content, the amorphous structure still maintained, the stability under light irradiation is improved at substrate temperatures higher than 300^0C and the hole drift mobility significantly increases up to 0.2 $cm^2V^{-1}s^{-1}$ at 300K.

The H_2 is decomposed at high microwave power in order to produce large amount of H atoms that not only promote the reaction in the gas phase but also strongly influence the surface reaction. Although the H contents remain high at high deposition temperature, it seems that more stable hydrogen complexes and lower density of weak Si-Si bonds are included. This explains why the remote hydrogen plasma samples at 400^0C have low urbach energy and defect density. These results seem contradictory, and it is difficult to establish whether the low H content or the changes in the microstructure are important for the increase of stability. Until now the unresolved principal problem is the identification of instability causes.

1.7 Effects of growth conditions

Electrical and optical properties of the films are determined by the growth chemistry during the deposition processes. The chemistry in plasma source is highly complex and not fully understood due to the formation of many sub-spices of radicals that are deposited on the substrate. Factors that affect the growth chemistry are chamber pressure, microwave power, substrate temperature, gas flow rates, and gas combinations.

As the pressure in the ECR-CVD reactor is reduced, the energy and the flux of Hydrogen ions increases causing the plasma density increase. Therefore, at low pressure, the growing film is subjected to increased ion bombardment and to increase a etching due to the higher density of hydrogen radicals. The larger energy hydrogen ions are able to

break weaker bonds and the result is a more homogenous film growth. A similar effect can be achieved by increasing microwave power. The etching effect removes the weak bonds and improves material quality.

The temperature of the substrate during the deposition process dramatically affects the quality of the film. Heating the substrate enhances the lateral mobility of the surface atoms and increase the desorption rate of hydrogen from the growth surface. This reduces an initial columnar morphology and microvoid content of the film, and decreases the contamination. Higher temperature yields a better crystal self-arrangement due to higher surface mobility. Amorphous films are grown at 300^0C to 400^0C.

The gas combination also dramatically affects the electrical properties of the film. Higher methane ratio gives higher carbon contents, which leads to a higher band gap, lower photo and dark conductivity, and lower growth rate due to higher energy bond of hydrogen carbon. The hydrogen dilution plays a very important role in improving the film quality and determining the growth rate. It was discussed in the section.

CHAPTER 2: SAMPLE FABRICATION

2.1 ECR-CVD Method

A new type of plasma being exploited for microelectronic processing is electron cyclotron resonant (ECR-CVD). ECR-CVD method was reported to have the advantage of being capable of producing high excitation plasma, which can be highly efficient for the breaking of the C-H and Si-H bonds in the reactant gases. This leads to the low defect density and interfacial damage in the films.

ECR plasma uses a perpendicular magnetic field along with an alternating electric field. The electric field increases the magnitude of the electron's velocity, and the magnetic field changes the direction of the velocity vector. If the frequency of the magnetic-field oscillation is set to the electron resonance frequency

$$\varpi = \varpi_c = \frac{eB}{m}$$

the amount of deflection causes by the magnetic field is just enough to turn the electron by 180^0 as the direction of the field changes sign. As a result the electron will move in a circle. This condition is called electron resonance. Electrons in resonant plasma gain energy throughout the circle if the mean free path is much larger than the circumference of the circle. This effect increases the power coupling efficiency and reduces the breakout field to as little as 10 V/cm. As with other magnetically enhanced plasma, the use of ECR dramatically increases the density of ions and free radicals in the discharge. If the process to be run depends on the ion flux from the plasma, an ECR will improve the rate at which the process occurs. For reasonable fields, the required cyclotron frequency is large, typically 2.45 GHz. An ECR system, therefore, requires the generation of high power microwave signals that coupled into the reactor. The microwave energy is typically carried by rectangular waveguides. The power is transmitted into the chamber through a quartz window. A condition of low reflected power is achieved by matching the source to the load.

The reactor used in this study is shown schematically in Figure 2.1. It consists of a microwave source operating at 2.45 GHz, which feeds power through a 3-stub tuner into a cavity. This multi screw tuner is used to match the source to the load through the

dielectric window, achieving a condition of low reflected power. The axial magnetic field to create the ECR condition is produced using two coils, and the relative position and magnetic field strengths are controllable by the operator.

The magnetic field needed for ECR resonance is about 875 Gauss for 2.45 GHz. Two DC power supplies (10V, 200A) are used to power the magnets. The position of resonant plain is set at about 20 to 30 cm away from the substrate.

The plasma gas is introduced into the microwave cavity near the microwave source end. Silane and methane are introduced near the substrate through a separate manifold. The typical pressures used for the growth are in the range of 5-10 mTorr. At these pressures, the excited H radicals have a long mean free path and they arrive at the substrate with significant energies.

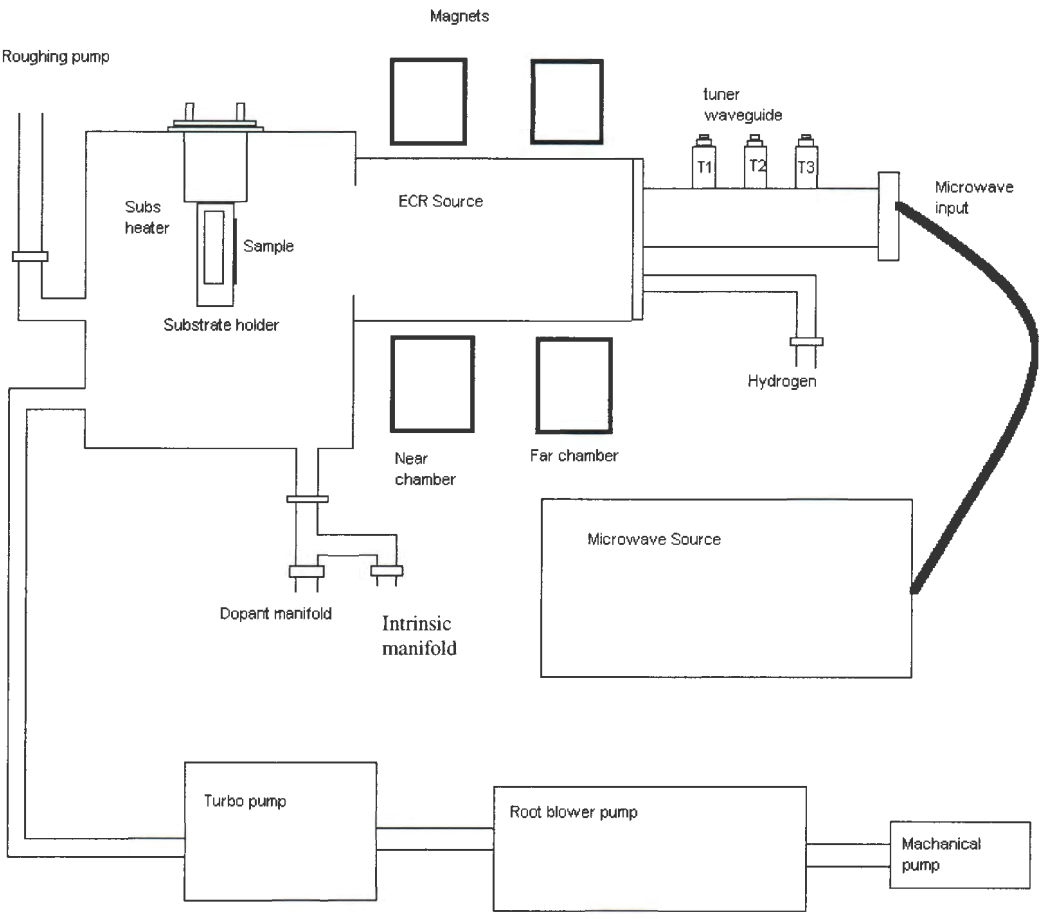

Figure 2.1: ECR system

2.2 Model of growth chemistry

Several chemical reactions and ionization can take place when dissociation of the precursor gases occurs. First, the hydrogen ions are created by an acceleration electron

$H_2 + e^- \rightarrow 2H^+ + 2e^- + e^-$

The electron can also break silane into radicals

$e + SiH_4 \rightarrow SiH_3 + H$

Silane (SiH_4) can be broken down into SiH_3, SiH_2, and SiH radicals.

$SiH_4 + H^+ \rightarrow SiH_3^* + H_2$

$SiH_3 + H \rightarrow SiH_2^* + H_2$

$SiH_2 + H \rightarrow SiH^* + H_2$

Similarly, methane (CH_4) can be broken down into CH_3, CH_2, and CH radicals. The rates of dissociation are different due to the differences in bond strengths.

This multi-species growth leads to a non-homogenous film that results in a material of poor quality. Therefore, low-temperature deposition requires carefully attention to plasma chemistry to ensure that only one of the radical structures is incorporated into the film growth.

The excess hydrogen ion forces the production of silyl and methyl radicals. Also, the excess hydrogen atoms will see the three Si-H bonds or C-H bonds and break them to form H_2 gas, allowing Si-Si, Si-C, and C-C bonds formed (Figure 2.2). Therefore, surface homogenization is achieved by deposition of SiH_3 and CH_3 radicals and H passivating any active sites. This process results in more homogenous growth.

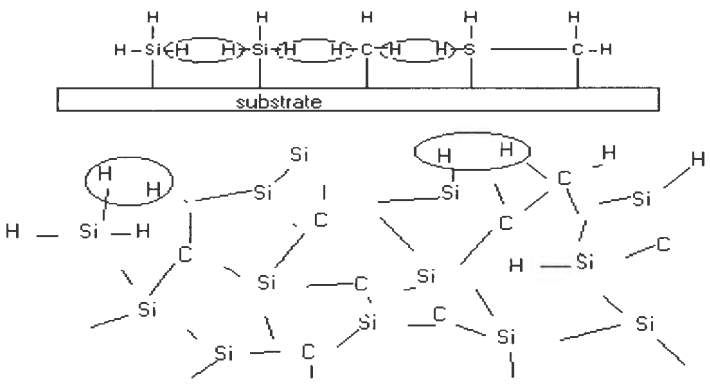

(a) Growth begin

(b) Continuing growth

Figure 2.2: Models of amorphous silicon carbide growth

2.3 Doping in amorphous silicon carbide alloy

Doping in a-SiC has been a subject of active research. Some works, based on the chemical equilibrium reactions between defects and dopants, set the basis for the understanding of doping in a-SiC[17]. Besides the desired shift of the Fermi level, doping affects the matrix network and produces bulk and surface effect. Doped a-SiC is used as *p* or *n* layers in *p-i-n* solar cell and the study of changes of the optical and electrical properties of this material during its doping is of great interest for the improvement of solar cell characteristics. The doped layers should be transparent (have a high bandgap) to minimize the optical absorption and have high conductivity to reduce parasitic series resistance of solar cell. To the first approximation, the variation of the open-circuit voltage of the solar cell follows the variation of build-in potential, although other factors limit the open-circuit voltage. Thus, for maximum solar cell conversion efficiency, the optimum doping level must be found to ensure a compromise between high conductivity and low absorption in the n or p layers.

It is known that hydrogenated silicon carbide thin films possess the properties of both wide optical bandgap and high conductivity. For a-SiC:H films, the introduction of the dopants into the amorphous network enables the control of electrical properties but at the same time change of optical bandgap. The decrease of optical bandgap has been reported by Sah and Lee to be due to the reduction of the hydrogen bonding to both Si and C atoms by the boron doping [18].

In order to dope amorphous silicon carbide n-type and p-type, phosphine gas (PH_3) and diborane (B_2H_6) are most commonly used, respectively. The problem of doping in amorphous silicon carbide become evident by considering the fact that atoms in the disordered structure are in three-fold coordination rather than four-fold as in crystalline silicon carbide. Doping in crystalline structures supplies holes and electrons due to an excess or a deficiency of electrons compared to the number of electrons necessary to form four-fold covalent bond. Since amorphous silicon carbide has some three-fold atoms, not all the impurity atoms contribute to doping effect. Doping in amorphous silicon carbide can introduce new defects, which could have significant influence in the optoelectronic properties of the materials.

2.4 Preparation of amorphous silicon carbide p-i-n devices

Single-crystal silicon carbide solar cells tend to be expensive and are limited to approximately six inches in diameter. A system powered by solar cells requires a very large area solar cell array to generate the required power. Amorphous silicon carbide solar cells provide the possibility of fabricating large area and relatively inexpensive solar cell system .

Amorphous silicon carbide has a very high optical absorption coefficient, so most sunlight is absorbed within approximately 1 μm of the surface. Consequently, only a very thin layer of amorphous silicon carbide is required for the solar cell. A typical amorphous silicon solar cell is a p-i-n device. Our amorphous silicon carbide is deposited on the stainless steel substrate. The n^+ and p^+ regions can be quite thin while the intrinsic region may be in the range of 0.2 to 0.25 μm thick. The energy band diagram for the thermal equilibrium case is shown in Figure 2.4(b).

A phosphorus doped n^+ layer is deposited on a cleaned substrate. It is about 0.3 μm, thick enough to reduce shunts arising from the rough substrate. The undoped i layer of thickness about 0.2 μm is deposited with the ratio of methane and silane which can give a desired bandgap. A buffer layer in then deposited to limit the diffusion of boron from next layer. Finally, boron doped p-layer of thickness of about 200 A is deposited. In order to allow most of the incident photons to reach i-layer, p-layer is usually chosen to be of higher band gap. The buffer i-layer is also need to assist in electron collection. A layer of 100 A of Cr is then deposited, followed by about 1000A of Al to make ohmic contacts (Figure 2.3).

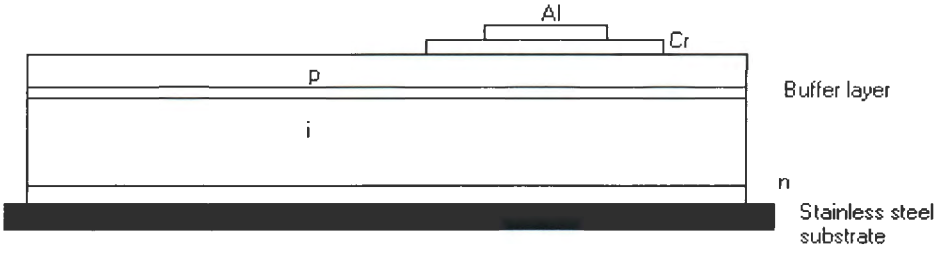

Figure 2.3: Cross section of pin device

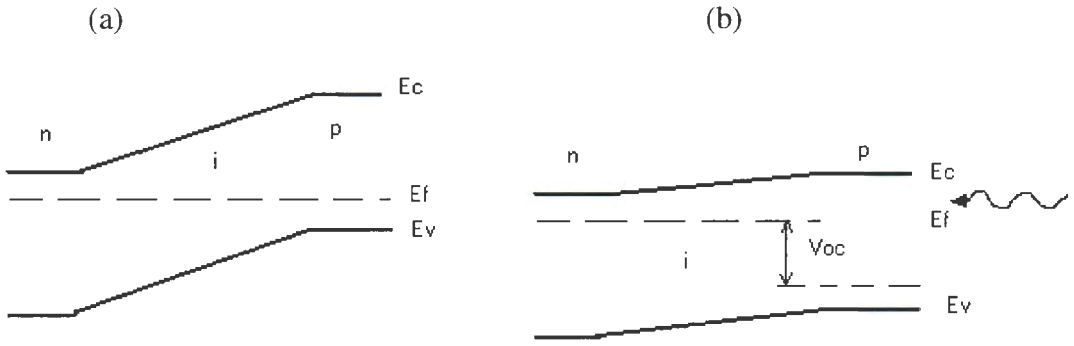

Figure 2.4: (a) energy-band diagram at thermal equilibrium, and (b) energy-band diagram under photon illumination of an amorphous silicon carbide PIN solar cell

2.5 Metallization

Electrical measurement on the films is done through chromium contacts, which have been deposited by thermal evaporation. The thermal evaporator system consists of a bell jar with resistively heated chromium rods and aluminum boat. A mask is placed in front of the film or device so that the metal contact is selectively deposited. The openings in the mask provide a length-width ratio of 20 for film. After the film or the device, which has the mask on it, is load into the evaporator chamber, the bell jar is pumped to a base pressure in the range of 3E-6 Torr before the evaporation is started. The chromium rods or aluminum boat is heated up by a DC bias applied voltage, then chromium or aluminum begins to evaporate. The chromium layer is deposited at an average of 5 Angstroms per second and the thickness is approximately 1000 Angstroms for film and 100 Angstroms for device, as measured by a thickness monitor inside the evaporator (Figure 2.5). The aluminum layer is deposited at an average of 20 Angstroms per second and the thickness is approximately 1000 Angstroms for the device. Silver paint is applied on top of the films chromium contacts to provide a good contacts to the metal probes. The conductive paint also helps to reduce contact resistance. The samples are then annealed at 180^0C for at least half hour.

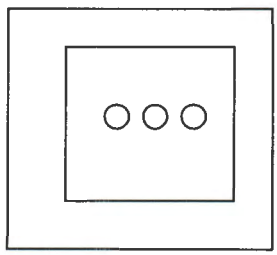

Figure 2.5: Chromium contacts

CHAPTER 3: CHARACTERIZATION TECHNIQUES

3.1 I-layer thickness

Since devices were deposited on stainless steel substrate, reflection data instead of transmission has to be used with spectro-photometric technique. Using the same equation of thickness, we could obtain the thickness of n and i layer, for the p-layer was much thinner than n and i layer. Then subtracting n layer thickness from (n + i) thickness, we obtained i -layer thickness.

A Lambda-9 dual beam spectrophotometer was used for investigations into the thickness, absorption coefficient and optical bandgap of the Amorphous Silicon Carbide then films. The thickness of the thin films and devices can be determined by the period of the oscillations in the transmission versus wavelength curve in the 600 to 2000 nm spectrum range (Figure 3.1).

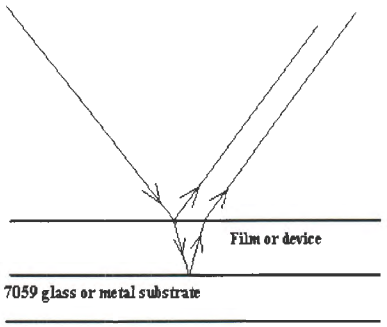

Figure 3.1: Thin film interference

The devices are grown on top of the stainless steel substrate. The thin films are grown on top of the Corning 7059 glasses. The glass is relatively very thick compared to the films, it does not contribute any interference effect, and therefore its effect is neglected.

A film or device is mounted perpendicular to the light rays. At the surface, the wave of reflection rays undergoes a phase change of 180^0. At the thin film-glass interfaces, the index of refraction of the film is greater than the index of refraction of the

glass, so the reflection does not cause a phase change. At the device-metal interfaces, the index of refraction of the device is smaller than the index of refraction of the metal, so the reflection does cause a phase change. The destructive interference of the film or constructive interference of device occurs at the wavelength such that

$$2t \sin\theta = m\lambda/\eta$$

where d is the thickness of the thin film, λ is the wavelength, η is index of refraction of the film, $\theta = \pi/2$, $\sin\theta = 1$, and m is an integer number.

The thickness can be determined by any two adjacent minimas (or maximas for devices) λ_1 and λ_2

$$2t \sin\theta = m\lambda_1/\eta = (m+1)\lambda_2/\eta$$

$$m\left(\frac{\lambda_1}{\eta} - \frac{\lambda_2}{\eta}\right) = \frac{\lambda_2}{\eta}$$

Solve for m and substitute to (1), we have

The thickness $$t = \frac{\lambda_1\lambda_2}{2\eta(\lambda_1 - \lambda_2)}$$

For film, if we use the peaks from transmission scan instead of reflection scan, λ_1 and λ_2 should be the maximas instead of the minimas. For devices, they are always the maximas. The refraction index of the film or the device is determined by solving for η in the expression:

$$Avg\langle R\rangle = \left(\frac{\eta - 1}{\eta + 1}\right)^2$$

where Ave<R> is the average reflection in the non-absorbing range. It is known that the index of refraction varies with wavelength; however, within this non-absorbing range the variance of reflective indices is small. As a result, the refraction index is assumed to be constant over the range of wavelength used. This assumption leads to a thickness accuracy of ± 0.1 μm.

3.2 Absorption coefficient, E_{04} energy and Tauc energy

3.2.1 Absorption coefficient and E_{04}:

The most direct and perhaps the simplest method for probing the band structure of semiconductors is to measure the absorption spectrum. In the absorption process, a photon of a known energy excites an electron from a lower to a higher energy state. Thus by inserting a thin film at the output of a monochromator and studying the changes in the transmitted radiation, one can discover all the possible transitions an electron can make and learn much about the distribution of states.

Fundamental absorption refers to band-to-band or to exciton transitions, i.e., to the excitation of an electron from the valence band to the conduction band. The fundamental adsorption, which manifests itself by a rapid rise in absorption, can be used to determine the energy gap of the semiconductor.

The absorption coefficient as a function of wavelength can be calculated using the following expressions for the absorption, reflection, and transmission as functions of the wavelength of the incident photons

$$A(\lambda) = \log\frac{1}{T(\lambda)}$$

$$T(\lambda) = [(1-R(\lambda)]\exp[-\alpha(\lambda)\, t]$$

where $A(\lambda)$ is the absorption, $T(\lambda)$ is the transmission, $R(\lambda)$ is the reflection, t is the thickness of the film, and $\alpha(\lambda)$ is the absorption coefficient. The absorption coefficient as a function of the wavelength can be calculated by combining the expression for $A(\lambda)$and $T(\lambda)$ and solving for the value of $\alpha(\lambda)$, which is found to be

$$\alpha(\lambda) = \frac{\ln 10 A(\lambda) + \ln[1 - R(\lambda)]}{t}$$

A plot of $\alpha(\lambda)$ versus E_{ph} provides visual information about absorption edge. The knee of the curve typically occurs around $\alpha(\lambda) = 10^4$ cm^{-1} which is denoted as E_{04} energy gap.

3.2.2 Tauc Energy:

Optical bandgap of amorphous thin films are frequently obtained from the Tauc equation

$$\sqrt{\alpha(\lambda)h\nu} = B(h\nu - E_{tauc})$$

where $\alpha(\lambda)$ is absorption coefficient, h is Planck's constant, ν is the radiation frequency, $h\nu$ is the radiation energy, equals to $1240/\lambda$ (eV), and B is a proportional constant. The E_{tauc} is determined by extrapolating the linear part of the absorption fitted by this equation to the photon energy axis, $h\nu$. Figures 3.2 and 3.2 are the examples of E_{04} and E_{tauc} energies.

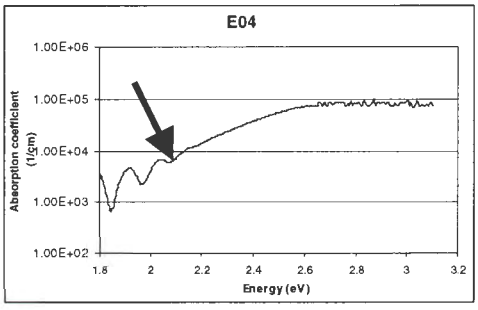

Figure 3.2: A sample of E_{04} energy

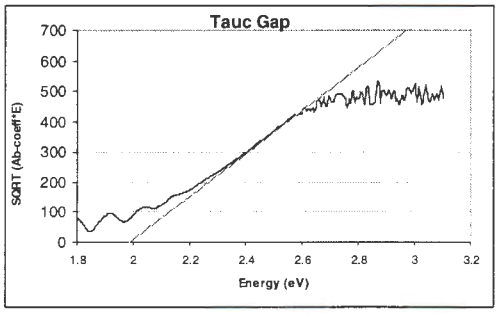

Figure 3.3: A sample of Tauc energy

3.3 Sub-bandgap absorption

The two-beam photoconductivity sub-bandgap absorption technique developed by Wronski, accurately probes the absorption sub-gap states below $\alpha=10^2$ cm^{-1}. Since the majority of films prepared by the ECR-CVD technique are less than 10 μm thick, thin film geometry limits the accurate determination of α from absorption and reflection data taken by the spectrophotometer to α's greater than 10^2 cm^{-1}. Another benefit of the two-beam sub-gap technique is that it enables the determination of absorption coefficients of film grown on non-transparent substrates such as stainless steel, polyamide, and molybdenum-coated polyamide.

This two-beam photoconductivity technique utilizes a DC light beam of high intensity to fix the quasi Fermi levels, while an AC light beam of low intensity probes the photoconductivity of the sample. The DC beam continuously creates electron-hole pair that keeps the traps filled and the occupancy of the mid-gap states constant. This fixed the lifetime of the photo-generated carriers. Meanwhile, the AC beam superimposes on

the DC beam and thus modulates the creation of addition electron-hole pair that can be detected by a lock-in amplifier. This photo-generated signal can be used to determine the absorption coefficient. To enhance the measured signal, a bias of 5 volts is placed across the sample to improve the transport of electron-hole pairs. The absorption coefficient is calculated at each wavelength by dividing the signal by a reference signal and multiplying by the quantum efficiency of the silicon reference detector.

In the experimental apparatus shown in the figure, the source is white light and the monochrometer is used to change the wavelength of the incident photons. The range of the wavelengths used in the measurement is from 400 nm to 1100 nm for SiC films. Chopping the output of monochrometer at 13.5 Hz creates the AC beam. This frequency produces a square wave and reduces the noise due to ambient light and 60 Hz power lines. High pass optical filters are added at 700 nm and 900 nm to reduce second harmonics from the monochrometer and to prevent photons of lower wavelengths from reaching the sample. The AC beam is collimated using two lenses and focused down onto the sample between the probe contacts with a mirror. Since the lifetime of electron-hole pairs is constant due to the DC light, the photocurrent corresponds directly to the absorption coefficient. Also, since the signal is detected with a lock-in amplifier, only the photocurrent corresponding to the chopper frequency is detected.

In this study, matching the curves is not important when determining the structure and quality of the material. What is important is the sub-gap data in the range between 1.0 to 2.0 eV. By plotting α versus energy, the trend of the curve can be compared to the trend of crystalline silicon carbide absorption curve. The crystalline trend is a rounded curve, while the amorphous trend has a curve that sharply drop to zero. Thus the shape of this curve is an electronic indication of the film's structure. The more closely the shape of the curve matches the crystalline curve the more likely the film is to consist of microcrystalline structures, otherwise it is amorphous.

3.4 Photo and dark conductivities

Photoconductivity is the change in the electrical conductivity when a material is exposed to electromagnetic radiation. An excess conductivity $\Delta\sigma$ appears if, under the action of absorbed light, the densities of the charge carriers n and p increase compared with their values at thermal equilibrium.

$$\Delta\sigma = e(\Delta n\mu_n + \Delta p\mu_p)$$

At low temperature the values Δn and Δp may be considerably higher than the corresponding equilibrium densities n_o and p_o. Under steady state conditions, the excess densities are equal to their rate of generation g multiplied by their average lifetime τ:

$$\Delta n = g\tau_n \text{ and } \Delta p = g\tau_p$$

The generation rate is governed by the quantum yield η, which is the number of electron-hole pairs generated by the absorption of photon.

The nonequilibrium charge carriers exist until they disappear by recombination which may occur though three processes: direct recombination of free electron and free hole, capture of an electron by a center in which a hole is localized, and capture of a hole by a center in which there is a bound electron. In steady state, a generation rate of carriers is equal to the recombination velocity.

Photosensitivity is the ratio of photo and dark conductivities. Amorphous materials absorb photon very efficiently. Thus amorphous materials will have a while large photosensitivity. To measure the photo and dark conductivies, the sample is placed on base and probes are connected to the sample contacts. A light source used to simulate the sunlight is an ELH lamp biased at 105 V, which is calibrated to the strength of the sun. The whole apparatus is enclosed in a chamber that prevents any photo generation of charge carriers when light source is off. There is a fan that keeps the sample at room temperature. The conductivity is determined by the expression:

$$\sigma_{d,\,ph} = \frac{WI}{LVt}$$

where W/L is the length to width ratio of the metal contacts, which is 20, t is the film thickness, V is applied voltage, and I is the measured current.

3.5 Activation energy

This characterization technique measures the activation energy due to the thermal excitation. Activation energy of an amorphous film can be used to directly determine the Fermi energy. An intrinsic material at low temperature should have the Fermi level half way between the tauc gap, and at room temperature the Fermi level may have a small fluctuation. Therefore, the activation energy can be good measure of how intrinsic the material is, which also indicates how good the deposition process was.

The temperature dependence of conductivity of a semiconductor material can be derived from the Fermi statistics for hole and electron as:

$$\sigma = \sigma_o \exp(-E_A/kT)$$

where $E_A = E_{c,v} - E_f$, k is Boltzman's constant, T is temperature in Kelvin, and σ is conductivity. From the equation above, measuring σ at different temperature and plotting $\log \sigma/\sigma_o$ versus 1/kT, we can obtain the activation energy from the negative of the slope. Amorphous films have a large negative slope.

Since σ_o is a constant, σ is proportional to measured current, the slope does not change if we plot current versus 1/kT instead of σ/σ_o.

$$\log(\sigma/\sigma_o)_1 - \log(\sigma/\sigma_o)_2 = \log[a*(\sigma/\sigma_o)_1] - \log[a*(\sigma/\sigma_o)_2]$$

where a is any constant.

In this technique, the substrate rests on the heater block inside an enclosed box. This eliminates any excitation due to photon absorption. To enhance the current, a bias of 100V is applied between the probes. The temperature ranges from 100^0C to 190^0C. The temperature is not allowed to exceed 200^0C as this prevents any change in the bond structure from occurring. Figure 3.4 is an example of activation energy measurement.

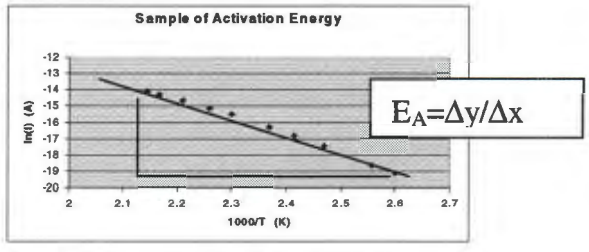

Figure 3.4: A sample of activation energy

3.6 Urbach energy

Urbach energy of valence band tails and mid-gap defect density are important parameters for determining the performance of amorphous material. Amorphous material has two different types of defects in its energy gap, the tail states near the conduction and valence bands, and the mid-gap defect states. In particular, the tail states limit the movement of level upon light excitation, and thereby provide a limit to open-circuit voltage that can be developed in an amorphous solar cell. The mid-gap states provide a very effective recombination-mechanism for excess carriers, and thus tend to limit the diffusion length of minority carriers, and hence fill-factors and open circuit voltage in solar cells.

The urbach energy of amorphous silicon carbide is calculated by the equation:

$$\alpha = \alpha_0 \exp[-\frac{E_g - h\nu}{E_{ur}}]$$

where $(E_g\text{-}h\nu)$ is the photon energy, α is the absorption coefficient, E_{ur} is the Urbach energy. Since for low αQE values are directly proportional to (αt), plotting $ln(QE)$ versus photon energy, we can obtain Urbach energy from the slope. A good material should have a low Urbach energy. Figure 3.5 is an example of Urbach energy measurement.

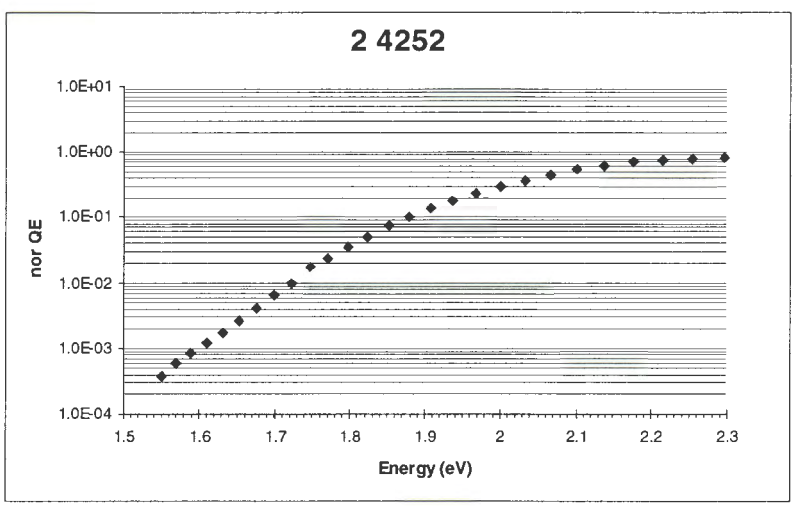

Figure 3.5: A sample of Urbach energy

3.7 Electron mobility-lifetime product

Electron mobility is a central parameter in characterizing carrier transport due to drift. The electron mobility is in fact a very important parameter, which plays a key role in characterizing the performance of devices. The lower the mobility of electron within a given semiconductor, the greater the number of motion-impeding collisions. To theoretically characterize the electron mobility, it is necessary to consider the different types of scattering events which can take place inside a semiconductor: phonon scattering, ionized impurity scattering, scattering by neutral impurity atoms and defects, carrier-carrier scattering, and piezoelectric scattering.

Phonon and ionized impurity scattering tend to dominate in a semiconductor. Phonon scattering refers to the collisions between the electron and thermally agitated lattice atoms. The coulombic attraction or repulsion between electrons and ionized donors or acceptor lead to ionized impurity scattering. The remaining scattering mechanisms are only important under certain conditions or enter indirectly into the over-all scattering analysis.

The carrier lifetime within a given material determines the response time of the R-G center interaction. The lifetime in turn is inversely proportional to the concentration of the dominant R-G center inside the material. The dominant R-G center is unintentional impurity incorporated into the material.

Previous researches have shown that a-Si:H alloying with carbon results in solar cells with inferior performance, as indicated by deterioration of the mobility-lifetime product mu*tau, measured by steady-state photoconductivity[7]. This is usually attributed to structural changes responsible for the increase in electron-capture cross-sections with illumination, i.e., a decrease in carrier lifetime τ. An alternative explanation is that the deterioration is due to long-range potential fluctuations that are produced in amorphous semiconductors by alloying or light soaking, causing a loss of mobility rather than lifetime. Steady-state photoconductivity cannot distinguish between these alternatives, because it does not determine μ and τ separately.

$$\sigma = \sigma_{photo} - \sigma_{dark} = q n_{electron} \mu = qG\tau\mu = qI\tau\mu/t$$

where G is number of photons absorbed per unit volume per second, I is the intensity of absorbed light and t is the thickness.

When the light passes through the material, the rate of light-intensity change is directly proportional to the incident light intensity.

$$\frac{dI}{dx} = -\alpha I$$

α is absorption coefficient of the material at the wavelength of incident light.

$$\frac{dI}{I} = -\alpha dx$$

$\Rightarrow$ $I(x) = I_o * \exp(-\alpha x)$

$\Rightarrow$ $I_{abs} = I_o - I_t$

$\Rightarrow$ $I_{abs} = I_o * [1-\exp(-\alpha t)]$

where *t* is the thickness of the film.

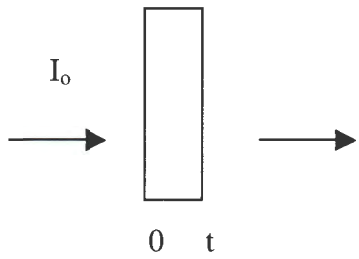

Figure 3.6: light absorbed

The mobility-lifetime product will be:

$\tau\mu = \sigma t / qI_{abs}$

where $\sigma = \sigma_{photo} - \sigma_{dark}$

3.8 I-V characteristic

The performance of a solar cell under illumination can be completely described by the current-voltage dependence. The ideal I-V characteristics of the solar cell (Figure 3.7) is given by:

$$J(V) = J_s \exp(\frac{qV}{nkT} - 1) - J_L(V)$$

where, J_L , which may be a function of voltage, is light induced current, J_S is the reverse saturation current, n is the diode factor, q is electron charge , k is Boltzman's constant, T is the temperature.

The short circuit current J_{SC}, which is the current of the cell illumination for V=0, is equal to $J_L(V)$, the photo-generated current, from the above equation. The photo-generated current depends on the spectra of the incident light, material response to the light and collection efficiency. It can be represented as:

$$J_L = q\int [1-R]Q(E)S(E)dE$$

where, R = reflection coefficient, S(E) = photon density spectrum of the light source, Q(E) = collection efficiency.

Open circuit voltage V_{OC} is determined by the ratio J_L/J_S and thus by the absorption and light generation process and the efficiency with which the charge carriers reach the depletion region.

Fill Factor (FF) is defined as follows.

$$FF = \frac{(VI)_{max}}{V_{OC} I_{SC}}$$

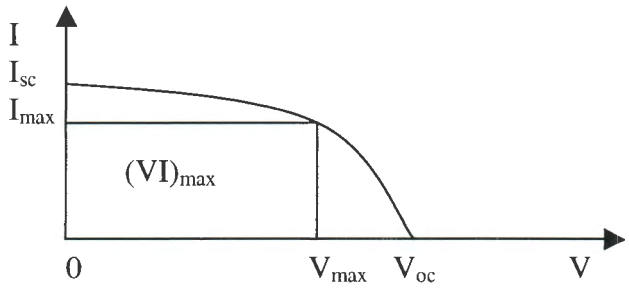

Figure 3.7: I-V curve

The reason this is important is understandable as the solar cell will be operated under conditions that give the maximum power output. It is easy to see that the more 'square like' the I-V curve, the larger the FF. FF is a good indication of the quality of the i-layer material, and how well the device is designed. A high FF requires low loss of photo-generated carriers in the i layer and at the interfaces, strong electric field in the i layer and a good ohmic contact. High quality amorphous devices have FF of about 65% - 75%. This value is less than that of crystalline solar cells since the mobility and diffusion length of holes in i layer is considerably less for amorphous materials.

A high V_{OC} requires efficient doping in the p and n layer, and also good interface. A high I_{SC} requires good material quality and optimal design of the cell to absorb and trap large number of incident photons.

The above three parameters determine the energy conversion efficiency η of the device by the following relation

$$\eta = \frac{(IV)_{max}}{\phi_{in}}$$

where, ϕ_{in} = total power of incident light.

3.9 Quantum Efficiency (QE)

QE is a diagnosis tool to characterize a semiconductor device. QE is defined as the number of charge carriers collected at a particular wavelength divided by the number of incident photons on the sample. This measurement provides information on how well the device absorbs photons at various wavelengths and how well the photo-generated carriers are collected under different bias conditions. The internal electric field is reduced under forward bias and the QE results provide details about how this reduction affects the collection of carriers. Also, any problem in the device design that may inhibit carrier collection such as hole traps at the p-i interface can be uncovered with QE measurements. Finally, dependence of QE at a particular wavelength as a function of bias can be used to obtain hole mobility lifetime ($\mu\tau$) product. If the QE is small for short wavelength photons (400nm - 550nm), this means that these photons are being absorbed in the p-layer, which in turn indicates p-layer may be to thick or have low band gap.
Our good QE plot is shown in the Figure 3.8, and the measurement setup is in Figure 3.9.

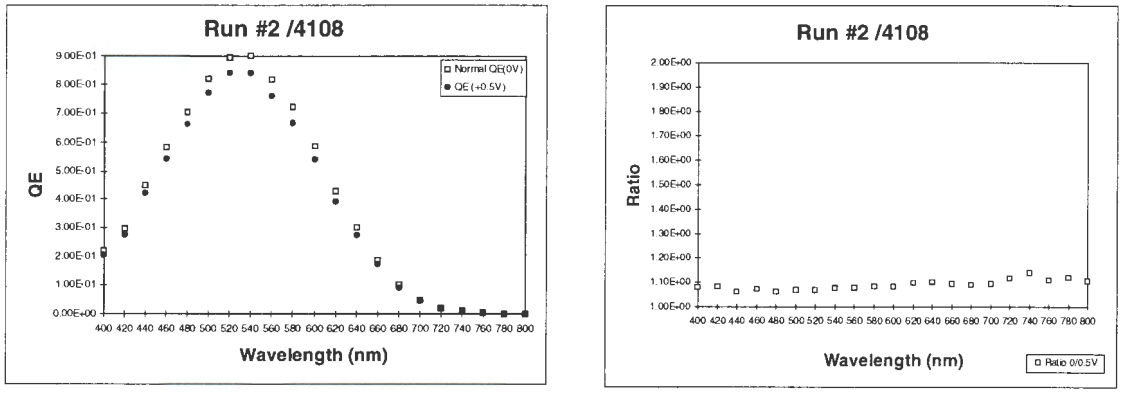

Figure 3.8: QE and QE ratio for a good a-SiC sample

QE(0)/QE(Va), where Va is applied voltage, provides information about the material quality. At forward bias the internal electric field is decreased for those carriers which are generated furthest from the collecting contact. If holes are the minority carriers, the reduction in QE at long wavelengths indicates a decrease in collection of holes. If the defect density is high, the electric field reduces significantly and for sufficiently high defects, the field could even collapse and reverse. A ratio of QE values

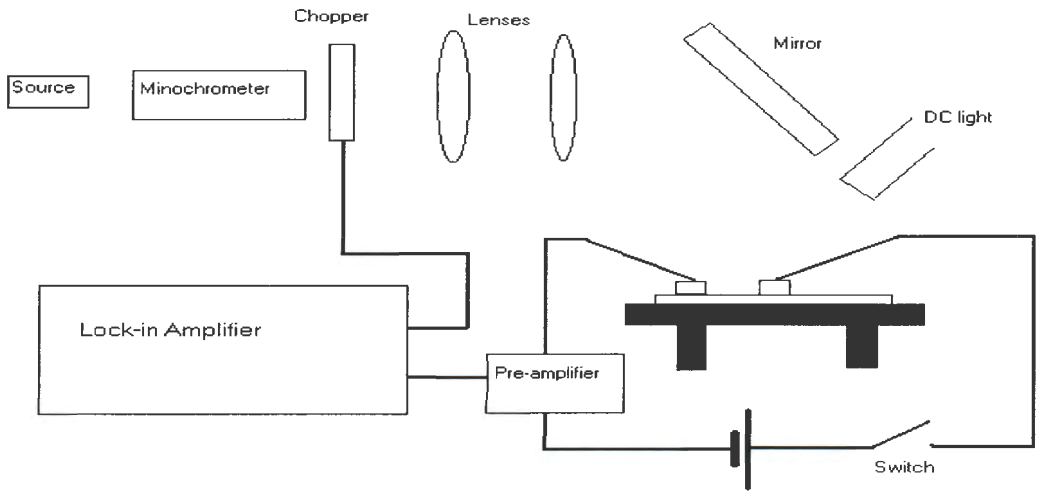

Figure 3.9: QE measurement setup

at zero and forward bias gives an indication of $\mu\tau$ of holes. Since the photon are incident on the p-layer, the lower energy photons are absorbed farther from the p-layer than the higher energy photons. Therefore, those photo-generated holes must drift farther across the i-layer before they are collected in the p-layer. If the QE ratio at these wavelengths is high, it indicates that the holes were being generated but were not being collected without the extra field-assist provided by the negative bias, which indicates a low $\mu\tau$ value of holes. Low QE ratio indicates a high $\mu\tau$ value. Also, if the ratio is high at shorter wavelength, the problem can be pinned on the p-layer or p-i layer interface.

As we have known, FF is a good indication of the quality of the i-layer material, and how well the device is designed and a high FF requires low loss of collection of photo-generated carriers in the i layer and at the interfaces, which means a lower QE ratio both at long wavelength and short wavelength. is required for high FF.

CHAPTER 4: EXPERIMENTAL RESULTS

4.1 Properties of amorphous silicon carbide material

4.1.1 Intrinsic amorphous silicon carbide

The influence of the substrate temperature on the growth of intrinsic a-SiC films has been investigated. Substrate temperature strongly affects the structure and electronic properties of hydrogenated amorphous silicon carbide. When the substrate temperature increases, then the photo and dark conductivities increase, the optical bandgap shrinks, the hydrogen content decreases, and the void fraction decreases.

Figure 4.1(a) indicates that the optical gap decreases as the substrate temperature increases. We kept the flow of silane at 10%, and varied the flows of methane from 10% to 30%. All of the samples were grown at pressure of 10 mTorr, 100% hydrogen dilution flow, and microwave power at 180W. Indicated substrate temperatures were varied from 250 to 450^{0}C. Real substrate temperature is about 30 to 50 ^{0}C below indicated temperature. Note that 100% hydrogen flow is equivalent to 70 sccm, 100% methane flow is equivalent to 31 sccm, and 100% silane flow is equivalent to 19 sccm. As the substrate temperature increases, the surface mobility increases allowing the reactive species to migrate to the correct site, the dihydride and monohydride content decreases, the void fraction decreases; therefore, the bandgap decreases. The films of higher substrate temperature have a lower subgap absorption corresponding to a low density of the midgap state.

Variation of the substrate temperature also dramatically affects the quality of the film. The higher quality films had the lower Urbach energy. Figure 4.1(b) shows that the samples grown by 15% methane flow, 10% silane flow, and temperatures at 300 to 400^{0}C, have a very good film quality. The Urbach energies of these samples are 45 to 50 meV. Those are the very good numbers for amorphous silicon carbide. This range of temperatures yields an optical gap from 1.95 to 2.05 eV, and photoconductivity and electron mobility-lifetime are in the order of 10^{-5} cm^2/V. Depending on the application, one can choose the appropriate substrate temperatures. The temperature of 300^{0}C is ideal if one wants to have films with higher bandgap (higher ratio of methane flow).

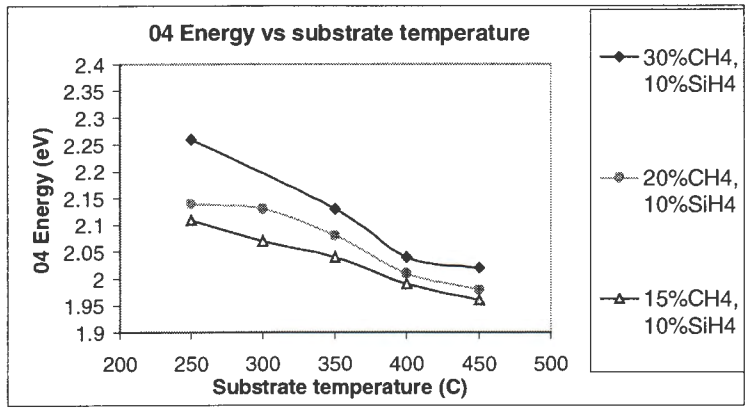

(a): The effect of substrate temperature on 04 Energy

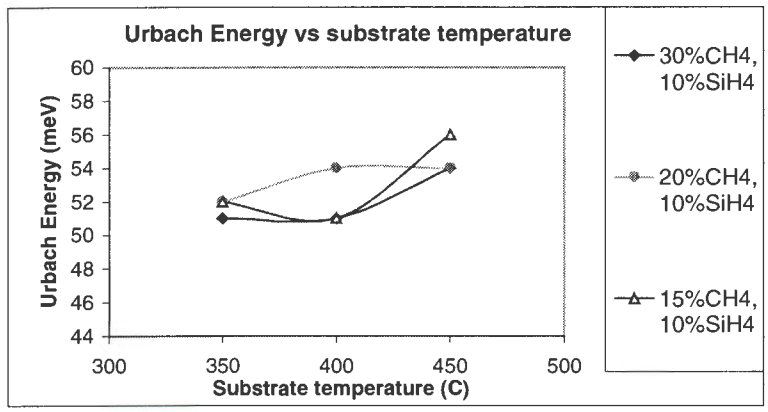

(b): The effect of substrate temperature on 04 Energy

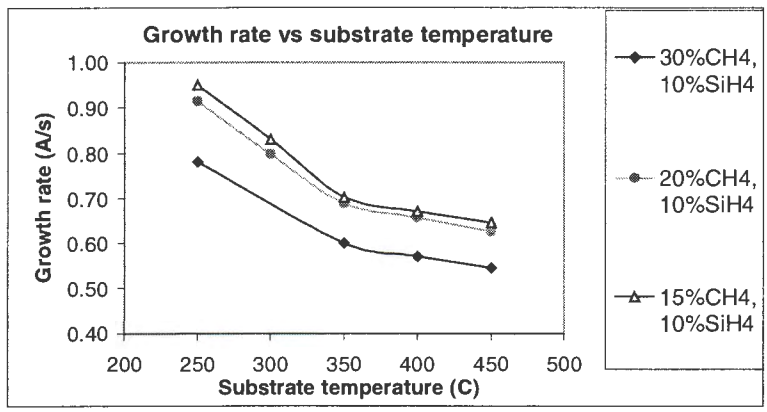

(c): The effect of substrate temperature on the growth rate

Figure 4.1: Effect of substrate temperature on the optical and electrical properties of intrinsic amorphous silicon carbide material

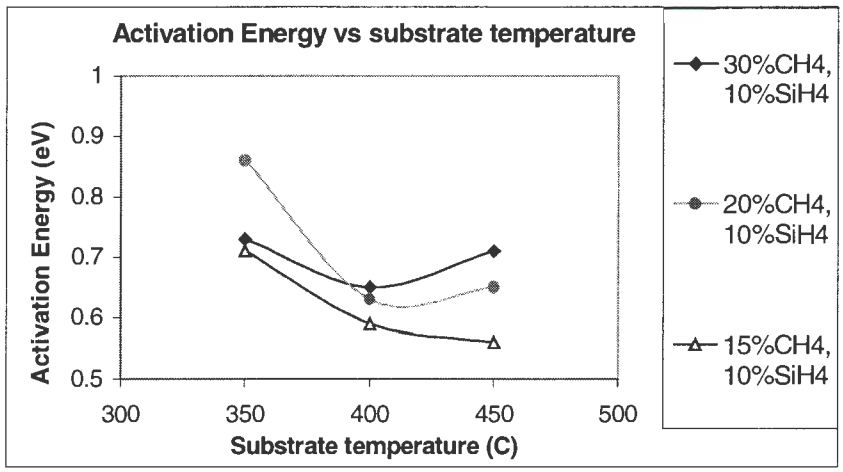

(d): The effect of substrate temperature on the activation energy

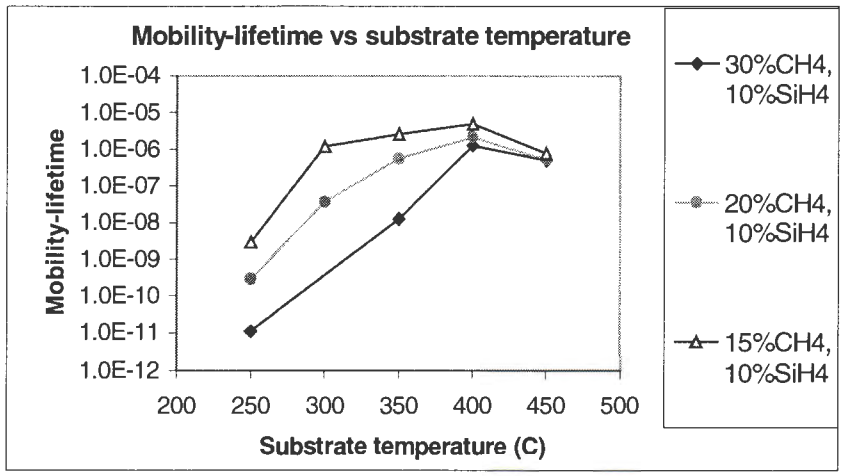

(e): The effect of substrate temperature on the $\mu^*\tau$ product

Figure 4.1 (continue): Effect of substrate temperature on the optical and electrical properties of intrinsic amorphous silicon carbide material

The Urbach energy of the samples that were grown at 350^0C are good for low carbon content materials. The film quality is also acceptable if the sample is grown at lower than 400^0C. This is the ideal condition for high conductivity and high mobility-lifetime product.

Photo and dark conductivities increase dramatically as the substrate temperature increases from 250 to 400^0C. The increase of photoconductivity is due to an increase of electron mobility-lifetime product (Figure 4.1(e)). The photoconductivity and electron mobility-lifetime product decrease when the substrate temperature increases from 400 to

450^0C, even though the bandgap decreases. We can see the relationship between mobility-lifetime produce and E_{04} energy in Figure 4.2. The small bandgap samples, which are grown at high temperatures, have both mobility-lifetime produce and E_{04} energy low. The substrate temperatures that exceed 400^0C give lower quality films and poor photovoltaic properties. In this case, the defects are dangling bonds left behind as hydrogen diffuses out of the film.

The growth rate changes significantly when the substrate temperature is varied (Figure 4.1(c)). The lower substrate temperature yields the higher growth rate. Amorphous silicon carbide has proved useful as a wide bandgap material in microelectronic devices. Alloying carbon into amorphous hydrogenate silicon increases the optical bandgap, but it also deteriorates the optoelectronic properties. Unfortunately, the increase of carbon content leads to the decrease in photoconductivity and the increase in paramagnetic-defect density.

Figure 4.1(c) also shows how the growth rate is affected by the ratio of gas flow. It is not surprising that the growth rate decreases as the ratio of methane flow increases, because it requires more energy to break a C-H bond than to break a Si-H bonds. The bond energy of a Si-H is about 320 KJ/mole and the bond energy of a C-H bond is about 410 KJ/mole; this suggests that most likely the SiH_4 molecules have higher dissociation efficiency than CH_4 molecules. Since the pressure is kept the same, the higher ratio of CH_4 should lead to a lower growth rate.

Carbon has a much higher bandgap than silicon; therefore, the sample with a higher ratio of carbon is expected to have a higher bandgap. Figure 4.3(a) shows that the films, which are grown by a higher methane flow, have wider 04 gap (and Tauc gap also). Thus, as expected, the methane flow has a strong influence on the optical bandgap. The optical gap is also affected strongly by substrate temperature.

Carbon content itself depends on a combination of the preparative condition. The carbon content comprises of the C-Si, C-C, and CH_x groups, each has its own distinctive core binding energy. The amount of components of each group strongly depends on growing condition. Therefore, the methane flow itself is not enough to determine the carbon content in the films.

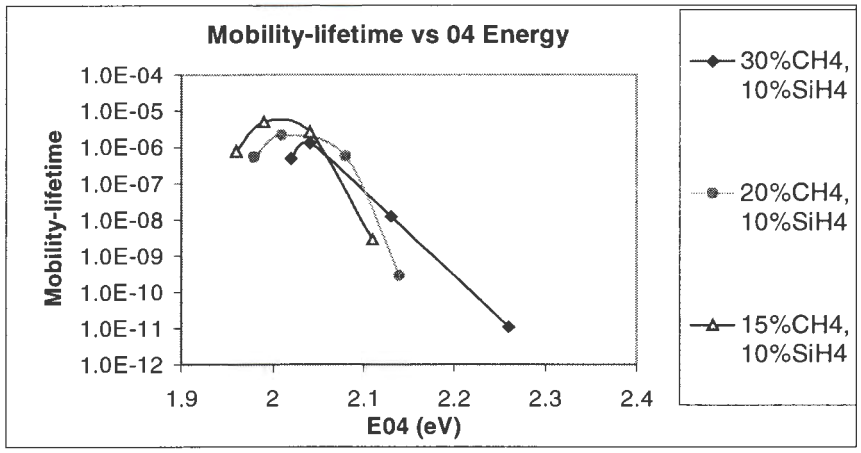

Figure 4.2: The dependence of $\mu^*\tau$ product on 04 energy

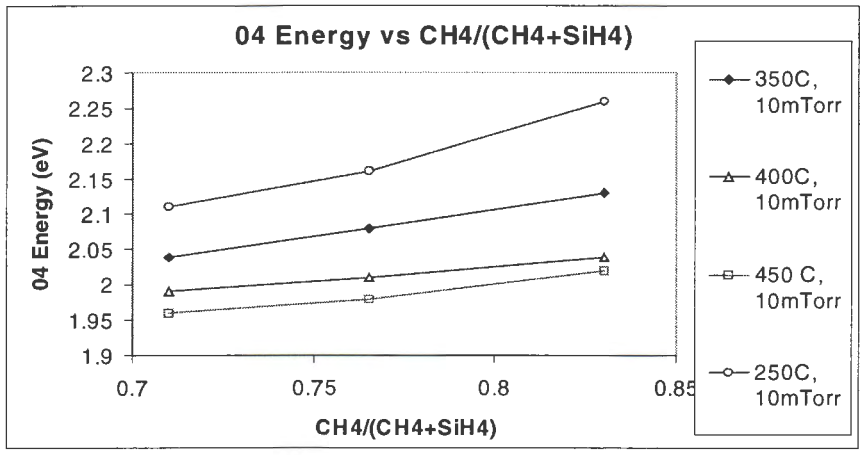

(a): Effect of gases flow on 04 Energy

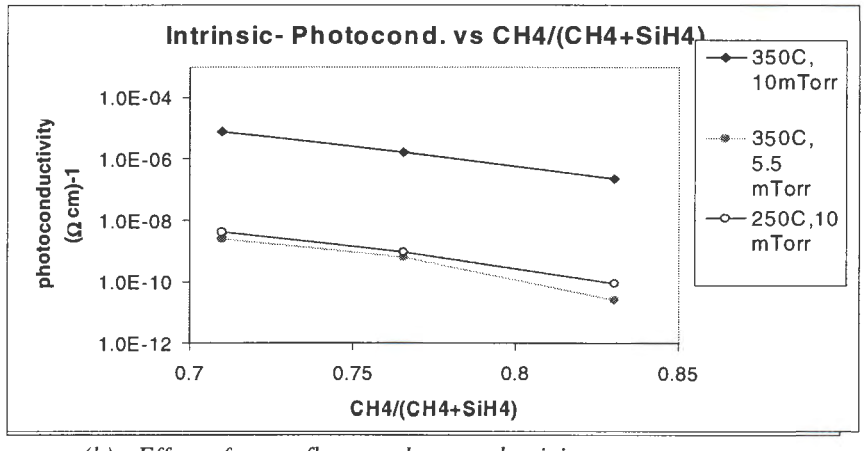

(b): Effect of gases flow on photoconductivity

Figure 4.3: Effect of gases flow on 04 Energy and conductivity of intrinsic a-SiC material

Films that have wider bandgap have either higher ratio of hydrogen or carbon, and both of them lead to the reduction of conductivity and mobility. Figure 4.1(e) also shows the photoconductivity and mobility-lifetime product as a function of the concentration of the source gases. Figure 4.3(b) shows that the photoconductivity decreases with the increase of optical bandgap, as well as the carbon content. Urbach energy depends on many other factors, other than the carbon content. Activation energy increases when the ratio of methane flow increases. Figures 4.4, 4.5, 4.6, 4.7, 4.8 show the relationships between E_{04} energy and electrical properties of the material. The electron mobility-

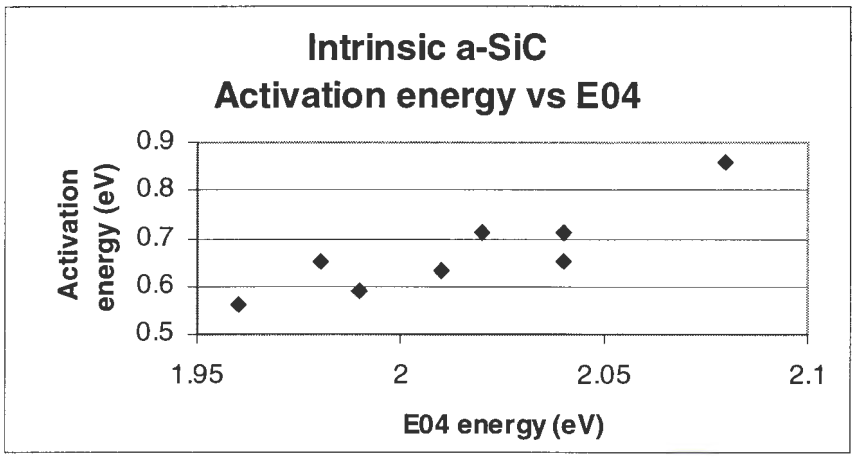

Figure 4.4: The relationship between E_{04} energy and Activation energy

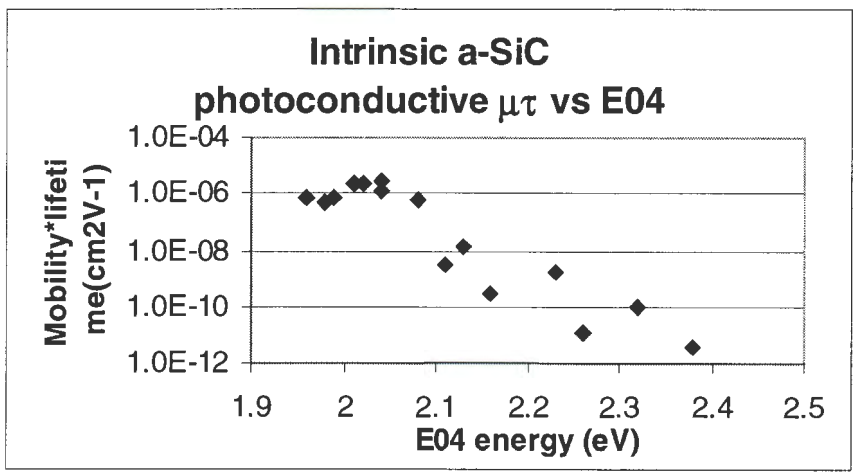

Figure 4.5: Relationship between E_{04} energy and photoconductivity

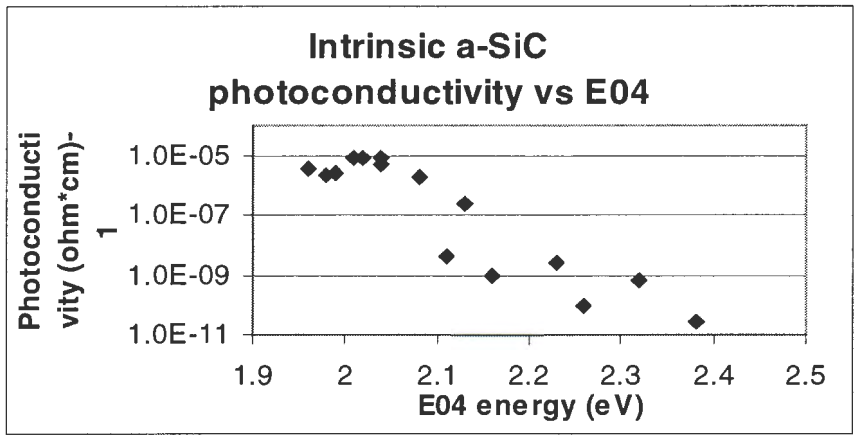

Figure 4.6: Relationship between E_{04} energy and photoconductivity

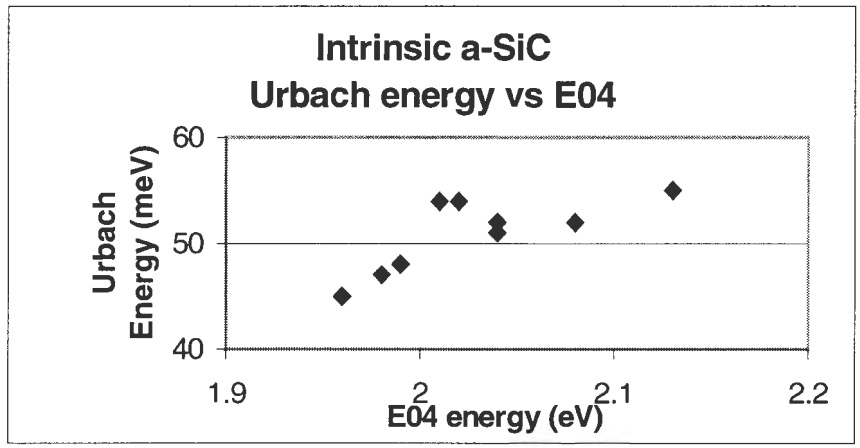

Figure 4.7: Relationship between E_{04} energy and Urbach energy

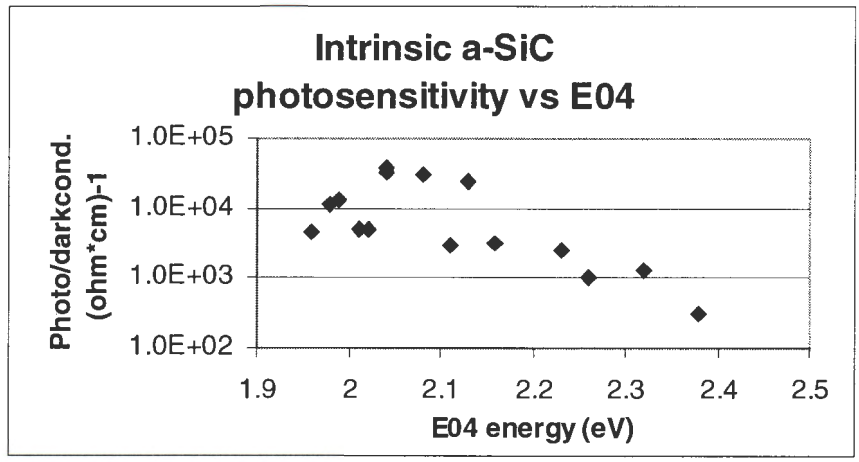

Figure 4.8: Relationship between E_{04} energy and photosensitivity

lifetime product and the Urbach energy of our material are significantly better than what have been reported in the literature. We will discuss in chapter 5.

4.1.2 Effects of phosphine and diborane doping on a-SiC

All the films reported herein were deposited using the ECR method from the mixture of SiH_4 and CH_4. The experiments of intrinsic a-SiC are performed with dilution flow of 70 sccm H_2, microwave power set at 180W, and chamber pressure of 10 mTorr. Methane, silane, phosphine, and diborone were varied to investigate the effects.

4.1.2.1 n-type doping by phosphine

Figure 4.9 compares the substrate temperature effects on n-type doped and undoped amorphous silicon carbide. Note that all the samples were grown at pressure of 10 mTorr, 70 sccm hydrogen dilution, 10% silane and 15% methane flows. The conductivity of both doped and undoped sample behaves the same way as the substrate temperature is varied. N-doped sample is not sensitive to light (no photoconductivity) because the Fermi level is already close to the conduction band.

Activation energy of n-type doped a-SiC is very low compared to the activation energy of an undoped one. Temperature does not seem to affect activation energy, but it dramatically affects 04 and Tauc energies.

The following graphs illuminate the dependence of n-type doped a-SiC growth rate, electrical property, and optical property on the gas flows. Unlike the intrinsic case, the growth rate of n-type doped a-SiC decreases dramatically as the methane flow increases. The growth rate of the doped samples decrease to half when the methane flow increase from 15% to 30%, meanwhile the change is not as dramatic for the undoped samples. So, we need to be careful with the thickness when we put more carbon in the n-layer.

In general, band gap energy of n-type doped a-SiC is not different from the intrinsic one. Figure 4.10(a) indicates that the magnitudes and variations of 04 and Tauc energies of n-type doped samples as a function of methane flow are not different from intrinsic cases. Even when the phosphine flow is varied, the bandgap is still unchanged. In Figure 4.10(b), we see that the growth rate changes significantly when the methane flow increases. The increase of methane flow also leads to the increase of activation

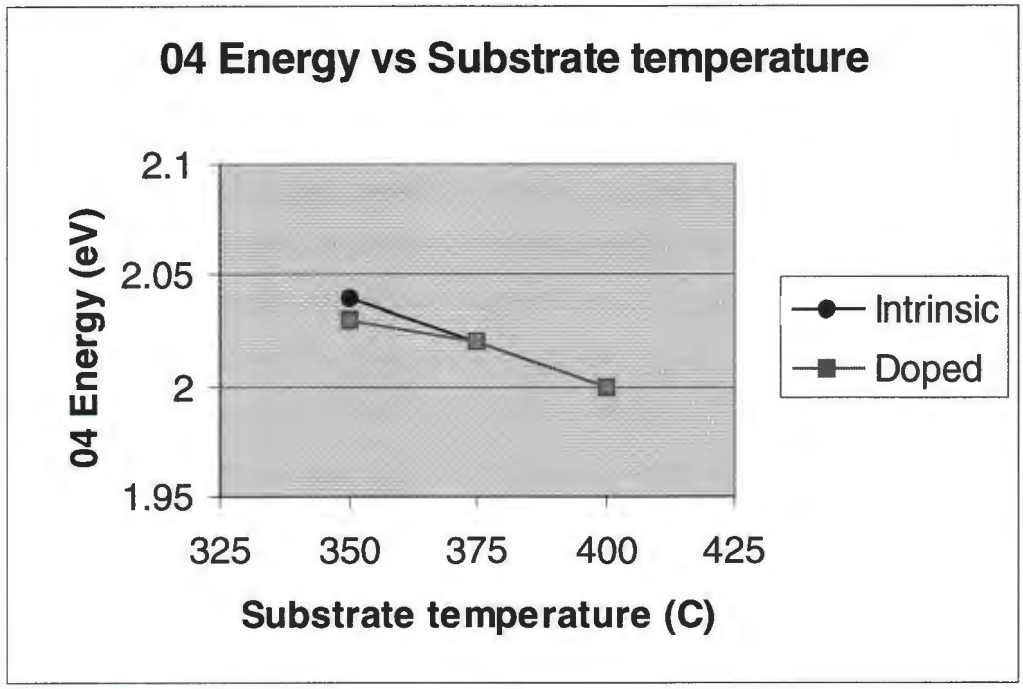

(a): temperature effect on 04 energy

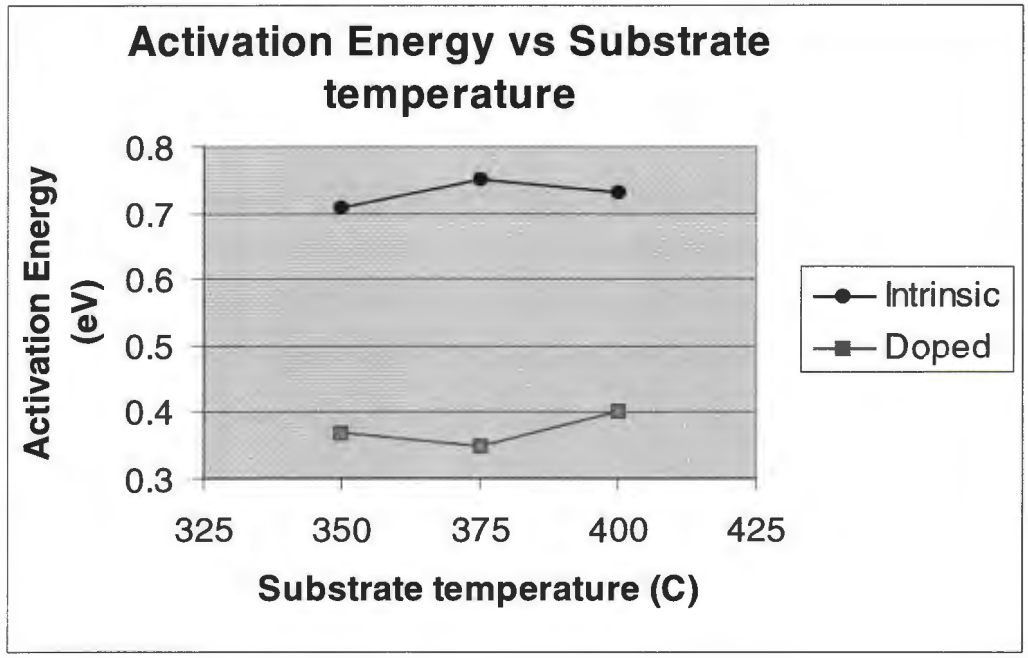

(b): temperature effect on activation energy

Figure 4.9: Temperature effect on 04 energy and activation energy

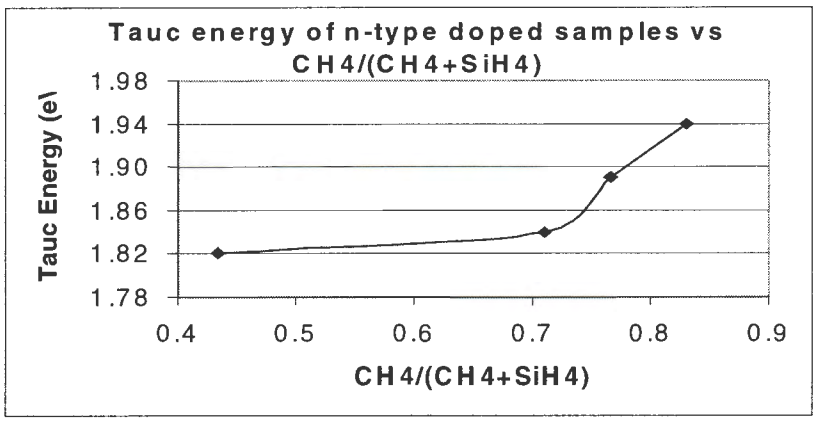

(a): Variation of 04 energies as functions of CH_4 flow

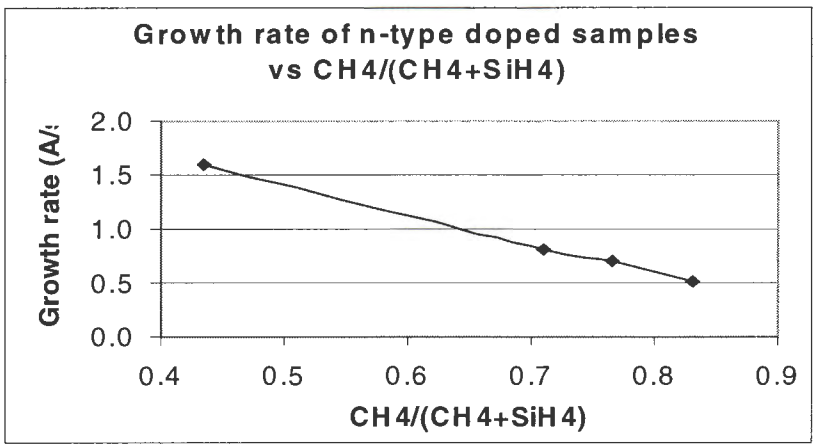

(b): Variation of growth rate as functions of CH_4 flow

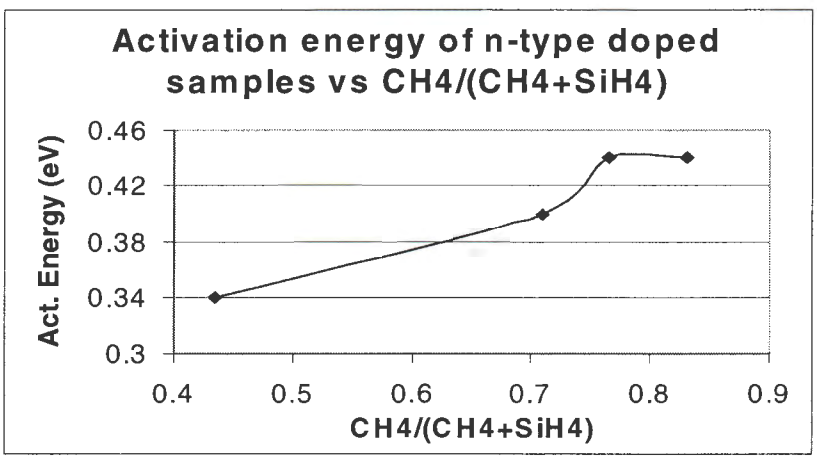

(c): variation of growth rate as CH_4 flow changes

Figure 4.10: Effects of gas flows on the bandgap, growth rate, and activation energy

energy (4.10(c)). Figure 4.11 indicates the relationship among E_{04} energy, activation energy, and conductivity of the n-doped material. In Figures 4.12(a) and (b), the change of the 04 and Tauc gaps as a function of phosphine flow, is shown to be less than .02 eV.

The variation of phosphine flow does not affect the conductivity, but it affects the growth rate. The large amount of phosphine consumes more available hydrogen provided by hydrogen dilution source. This makes more H-deficient sites which prevents the surface diffusion of SiH_3 and CH_3 radicals from finding their energetically favorable sites. Therefore, the deposition rate decreases as the phosphine flow increases.

4.1.2.2 p-type doping by diborane

Substrate temperature affects the structure and electronic properties of doped hydrogenated amorphous silicon carbide as well as of intrinsic hydrogenated amorphous silicon carbide. Where substrate temperature increases, photo and dark conductivities increase, the optical bandgap decreases, the hydrogen content decreases, and the void fraction decreases.

We kept the flow of silane at 5%, and varied the flows of methane from 10% to 30%. All of the samples were grown at pressure of 10 mTorr, hydrogen dilution flow of 100%, diborane flow of 40%, microwave power at 180W. Substrate temperatures were varied from 100 to 400^{0}C. Note that 100% hydrogen flow is equivalent to 70 sccm, 100% diborane flow is equivalent to 20 sccm of 1% B_2H_6/H_2 mixture, 100% methane flow is equivalent to 50 sccm, and 100% silane flow is equivalent to 64 sccm.

Figure 4.13(a) indicates that the optical gap decreases as the substrate temperature increases. Figure 4.13(b) shows that the growth rate changes significantly when the substrate temperature varies. The lower substrate temperature yields the higher growth rate. The temperature effect of the p-doped a-SiC has some differences from the temperature effect of intrinsic a-SiC. Surprisingly, the growth rate of the low-carbon-content samples jump up at the substrate temperature of 350^{0}C.

Conductivity increases dramatically as the substrate temperature increases from 100 to 300^{0}C. When the substrate temperature excesses 300^{0}C, the conductivities of the samples which have high carbon contents (high methane flow rate) decrease, meanwhile the conductivities of the samples which has low carbon contents continue to increase.

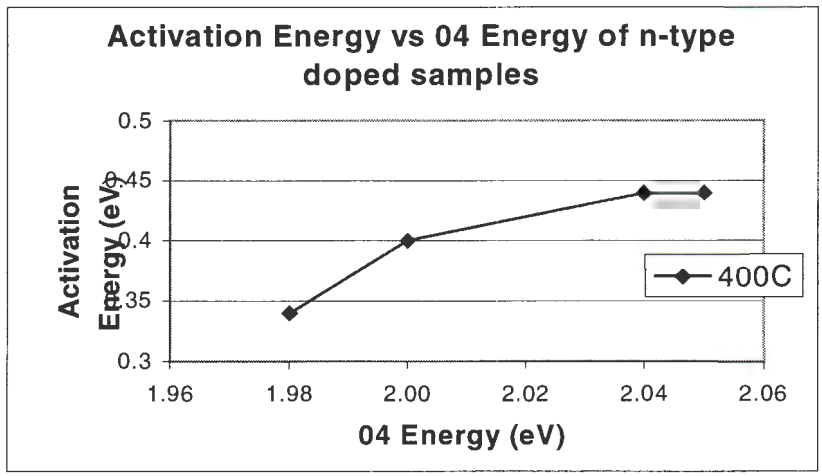

(a): Activation energy vs 04 energy

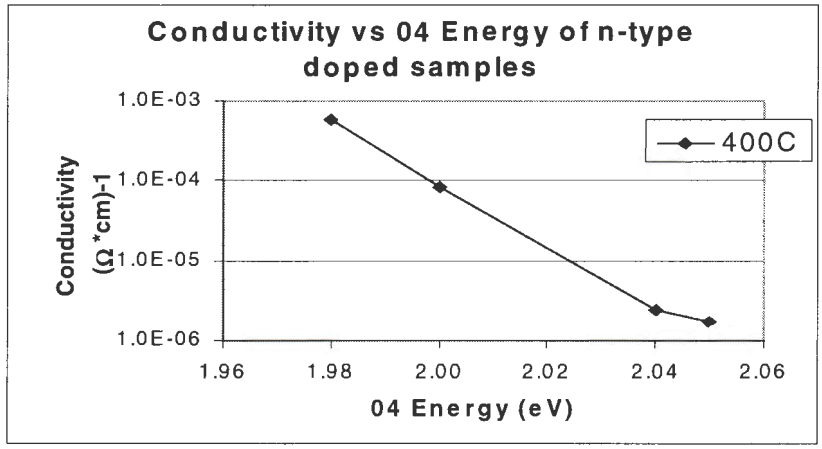

(b): Conductivity vs 04 energy

Figure 4.11: n-doped - relationship between E_{04} and activation energy or conductivity

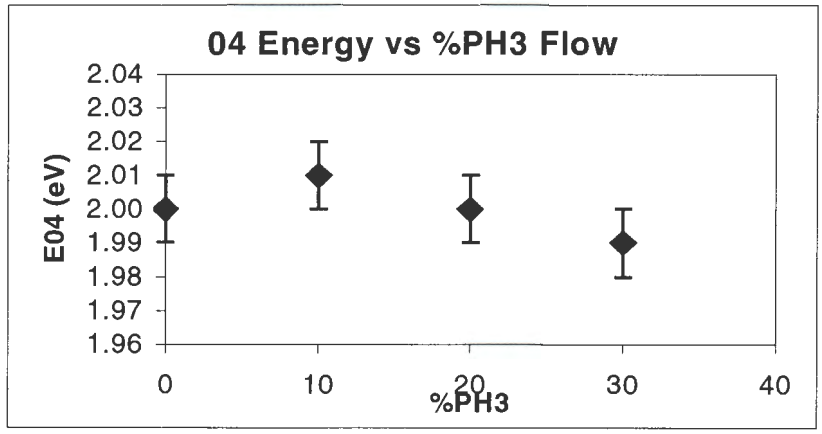

(a): variation of 04 as PH_3 flow changes

Figure 4.12: Effect of PH_3 flow on electrical properties and growth rate.

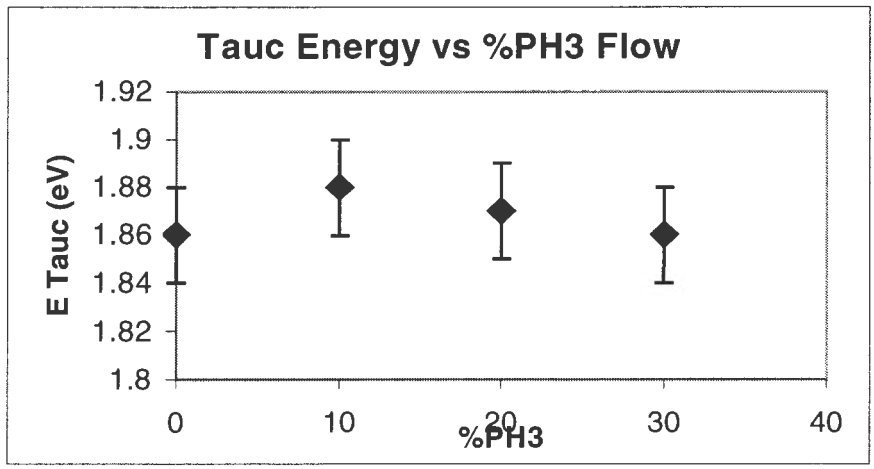

(b): variation of Tauc as PH_3 flow changes

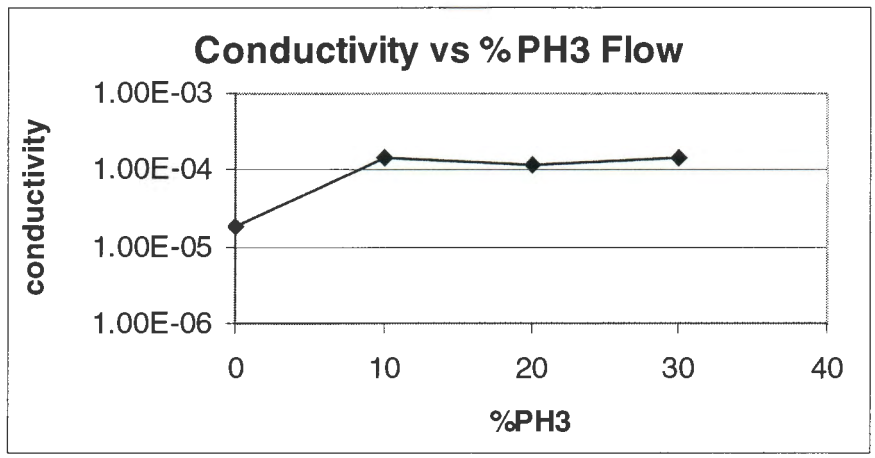

(c): variation of growth rate as PH_3 flow

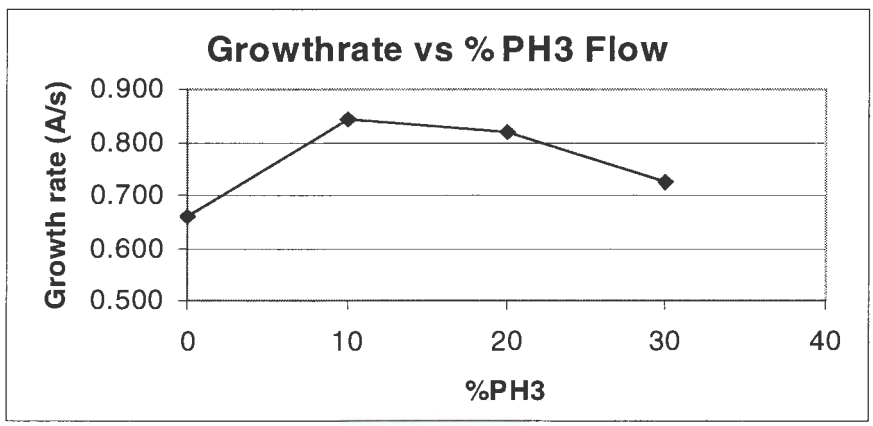

(d): variation of conductivity as PH_3 flow

Figure 4.12 (cont.): Effect of PH_3 flow on electrical properties and growth rate.

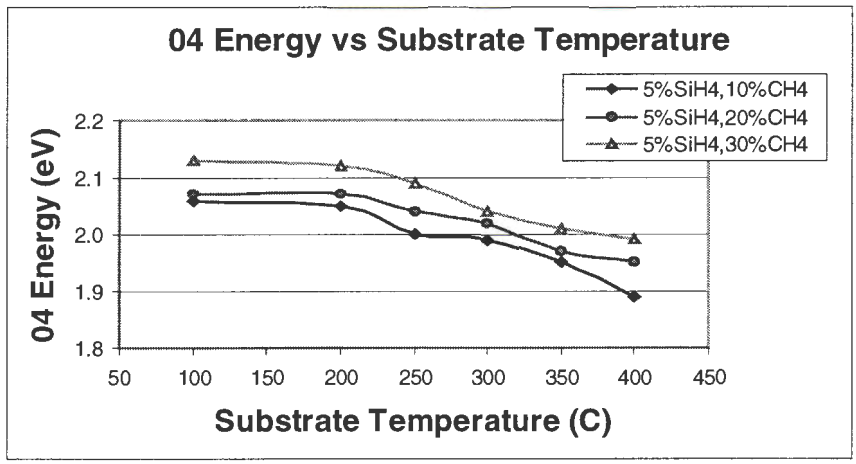

(a): Effect of substrate temperature on 04 Energy (p-doped)

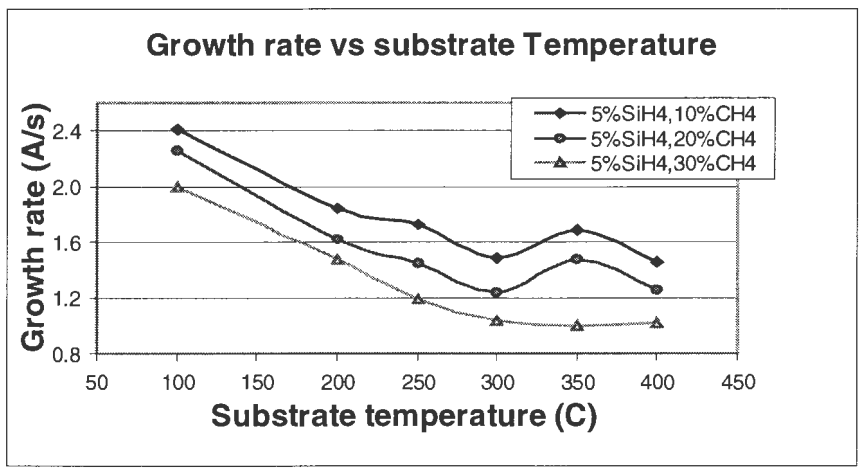

(b): Effect of substrate temperature on the growth rate (p-doped)

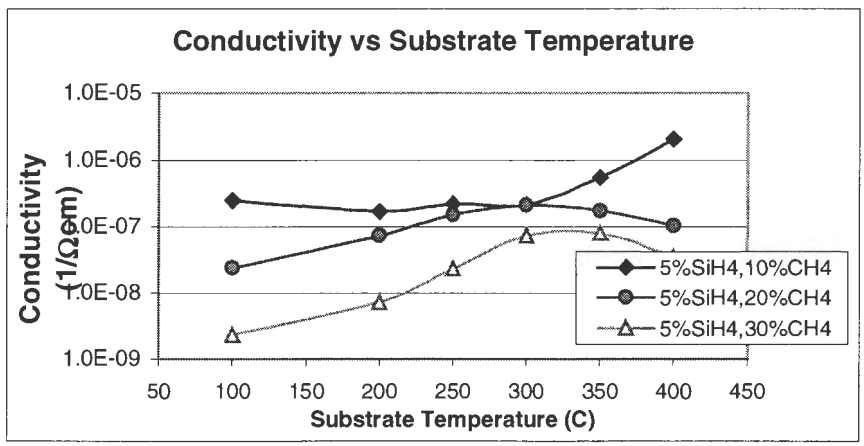

(c): Effect of substrate temperature on conductivity (p-doped)

Figure 4.13: Effect of substrate temperature on bandgap, conductivity and growth rate

The reason for that is the bandgap decreases as the substrate temperature increases. The wider bandgap samples have the lower conductivity. As the substrate temperature excesses 300^0C, the conductivity decreases instead of increasing.

The bandgap of p-doped amorphous silicon carbide is as wide as the bandgap of intrinsic one. Although alloying carbon into a-Si increases the optical bandgap, it also deteriorates the electrical properties. The most significant point is the decrease in conductivity with increasing carbon content. The activation energy also increases with the increase of carbon content.Figure 4.13(b) also shows that the growth rate is affected by the ratio of gas flow. It is not surprising that the growth rate decreases as the ratio of methane flow increases, because it requires more energy to break a C-H bond. Since the pressure is kept the same, the higher ratio of CH_4 should lead to the lower growth rate.

Carbon has a much higher bandgap than silicon. Therefore, the sample with higher ratio of carbon is expected to have higher bandgap. Figure 4.14(a) shows that the films which grown by higher methane flow have wider bandgap. Thus, as expect, the methane flow has fairly strong influence on the optical bandgap. The optical gap is also affected strongly by substrate temperature.

Films that have wider bandgap have either higher ratio of hydrogen or carbon, and both of them lead to the reduction of conductivity. Figure 4.14(b) shows the conductivity as a function of the source gas concentrations. We discover a very useful property of p-doped amorphous silicon carbide in Figure 4.14(c). The conductivity does not decrease dramatically when the bandgap increase due to the decrease of substrate temperature. The plots shift to the right instead of shifting to the lower right. Therefore, we can make the films that have both bandgap and conductivity high by lower the substrate temperature. With 5% silane and 10% methane flow rates, the conductivity is kept unchanged even when the bandgap increases from 1.97 to 2.07 eV by the variation of substrate temperature from 300^0C to 100^0C. It seems to be that 100^0C is the lowest substrate temperature we should make. Otherwise, the conductivity decrease but the bandgap does not increase if we continue to decrease the substrate temperature. Figures 4.15, 4.16, 4.17 show the relationships among E_{04} energy, activation energy, and electrical properties of the p-doped a-SiC material.

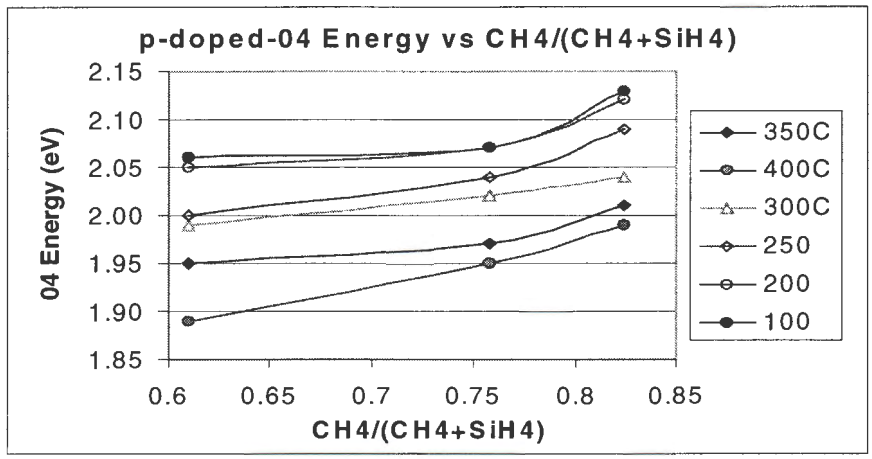

(a): Effect of gas ratios on E_{04} Energy

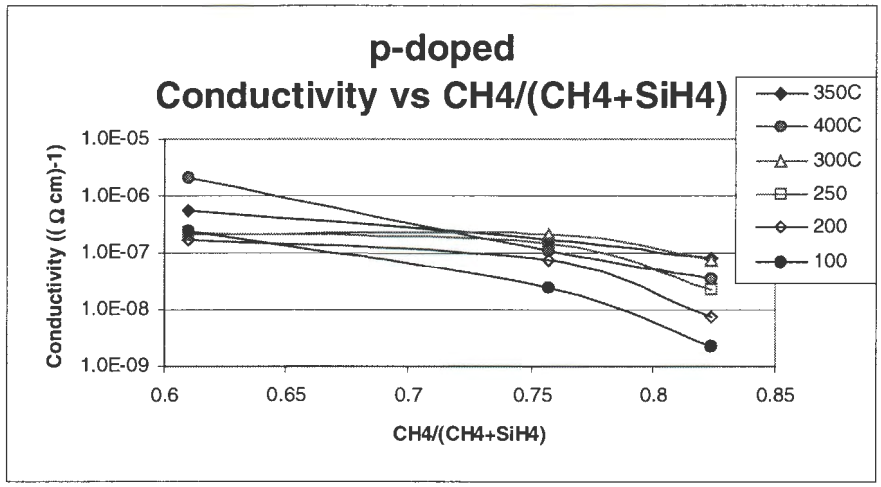

(b): Effect of gas ratios on conductivity

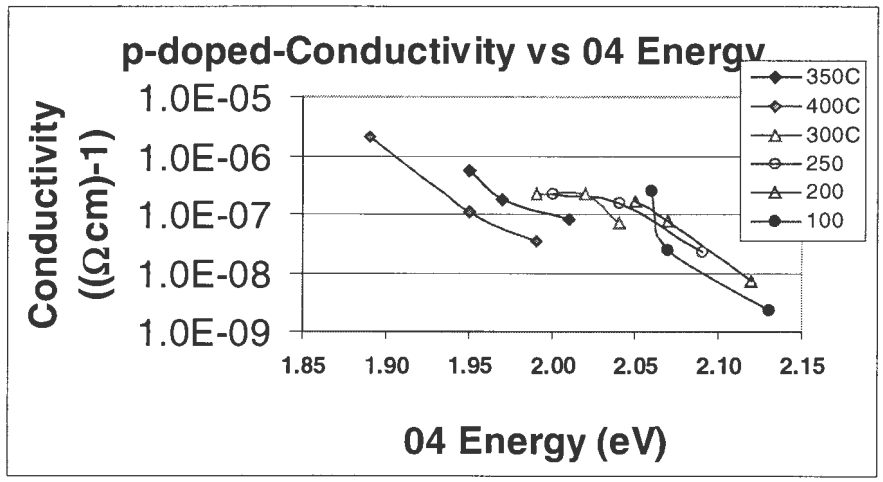

(c): Relationship between conductivity and E_{04} energy

Figure 4.14: p-doped - Effect of gas flow ratios on electrical and optical properties

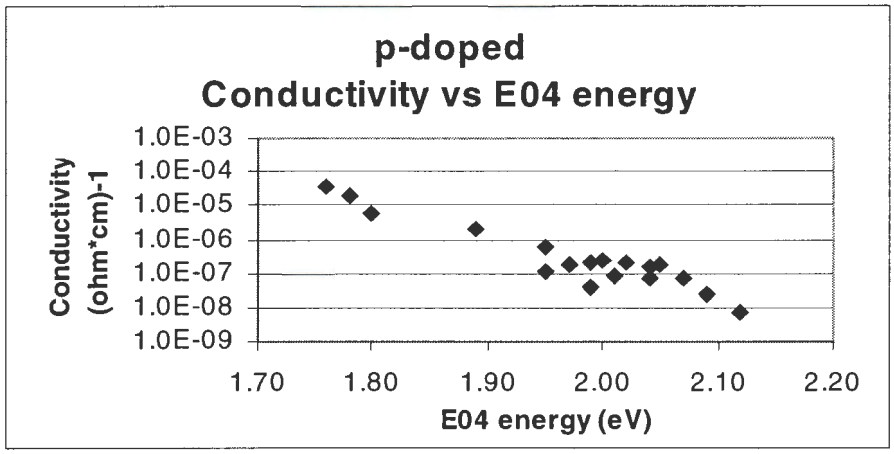

Figure 4.15: Relationship between conductivity and E_{04} energy

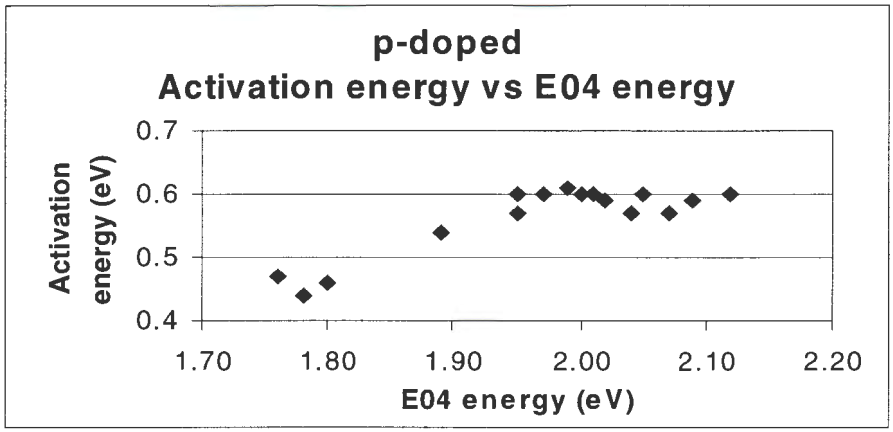

Figure 4.16: Relationship between activation energy and E_{04} energy

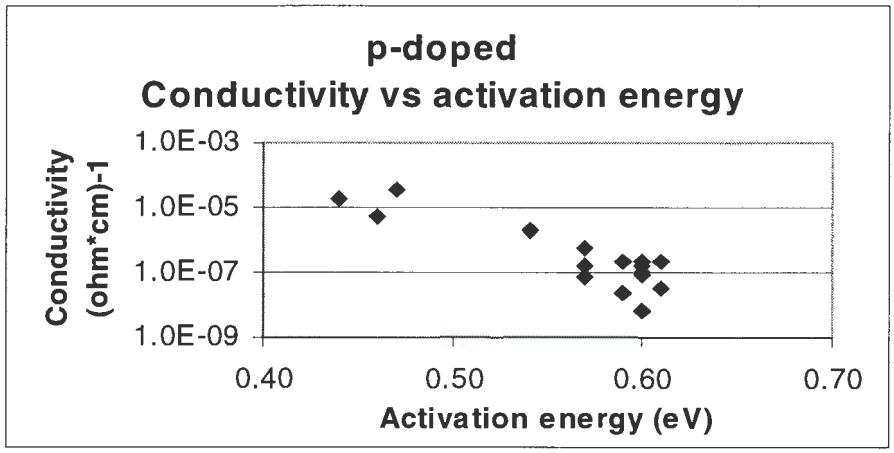

Figure 4.17: Relationship between conductivity and activation energy

4.2 Experimental results for amorphous silicon carbide solar cells

Amorphous silicon carbide solar cells yield a high open-circuit voltages as well as a high fill factor. The parameters which give good amorphous silicon carbide films were used for making amorphous silicon carbide solar cells. As we mentioned in the experimental results for amorphous silicon carbide material, the substrate temperature of 300 to 350^{0}C yielded very good film quality. Therefore, this range of temperature was chosen to make the intrinsic layer of amorphous silicon carbide cells. This range yields high bandgap, acceptable conductivity and mobility-lifetime product. The hydrogen dilution was kept at 40 sccm. The silane flow rate was varied from 2 to 4 sccm (10 to 20% of total flow). The methane flow was varied from 1.5 to 6.0 sccm. This was 5 to 20% of the total flow. The microwave power was kept at 150W, and the chamber pressure was kept at 10 and at 15 mTorr. The thickness of the i-layer was kept at about 0.2 μm.

The n^+-layer of our solar cell was amorphous silicon or silicon carbide. The bandgap of the n^+ -player was slightly higher than the bandgap of the i-layer. The p-layer was made of three thin layers. Because the p-layer had higher bandgap than the i-layer, the mismatch would cause a decrease of the collection of holes at the p/n interface. This problem had be solved by introducing a thin grading buffer between the p and i-layer.

The temperature for making p-layer was chosen to be 180^{0}C. The reason for using 180^{0}C is so that B_2H_6 does not thermally decompose. As said in the previous part of the p-doped material that this temperature can yield high bandgap (2eV) and the conductivity is also high. The pressure for making the p-layer was kept at 10mTorr, and the microwave power was 180W.

A microcrystalline (μc) p-layer was coated on top of the amorphous p-layer. Crystalline Si was an indirect transition material, so its coefficient of absorption was low. When the microcrystalline phase was mixed with the amorphous phase, the absorption coefficient was decreased. The number of photons reaching the i-layer was therefore increased because of the reduction of absorption loss in the p-layer. Finally, another amorphous p-layers were coated on the top of μc layer.

The i-layer was deposited at 10 mTorr and at 15 mTorr. The devices, which were grown at 10 mTorr, had better quality than the ones at 15mTorr (Figure 4.18). The low-deposition pressure increased the mean-free path, allowing more radicals to survive the transit from the plasma region to the surface. Therefore, the growth rate increased significantly at the low-deposition pressure.

The photovoltaic properties of amorphous silicon carbide solar cells are strongly influenced by the substrate temperature during deposition. For substrate temperatures of 250^0C or lower, the devices exhibit very poor photovoltaic properties due to large defect densities. Consequently, other electronic properties such as photoconductivity are also adversely affected by the short recombination lifetimes. The defect formed in a-SiC films and devices at substrate temperatures of 250^0C or lower may be associated with the dihydride or trihydride groups.

As we mentioned in the last section when we discussed about films, poor photovoltaic properties will also result if the substrate temperature is higher 400^0C. In this case, the defects are caused by the dangling bonds left behind as hydrogen diffuses out of the film.

Efficient a-SiC solar cells can only be made in the range of substrate temperature between 300 and 400^0C, and we have found that 350^0C is the best choice for the deposition pressure of 10 mTorr. Figure 4.19 indicates that for this choice of substrate temperature, the ratio of $CH_4/(CH_4+SiH_4)$ should be 0.7 to be able to get a best device (V_{os}=0.91, FF=0.71). If we choose the substrate temperature of 300^0C, the ratio of $CH_4/(CH_4+SiH_4)$ should be 0.6 to get the most optimal device (V_{os}=0.90, FF=0.70) (Figure 4.18). The reason for this is the sample that is grown at 350^0C have lower

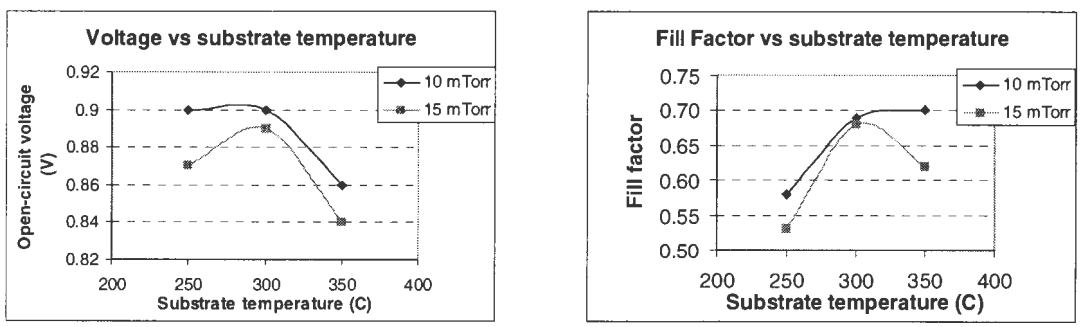

Figure 4.18: Effect of substrate temperature on photovoltaic properties ($CH_4/(CH_4+SiH_4)$=0.6)

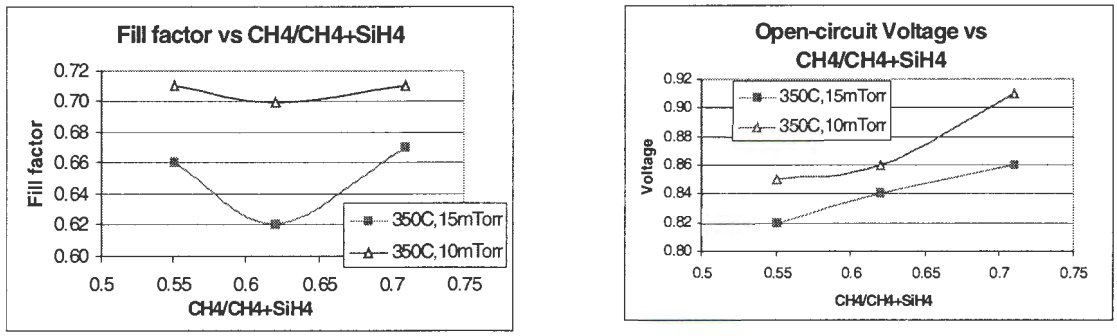

Figure 4.19: Effect of ratio of methane flow on photovoltaic properties

bandgap due to higher level of crystallinity, there for the carbon content should be higher to keep the bandgap high. Figures 4.20 and 4.21 show that the two samples (350^0C, $CH_4/(CH_4+SiH_4)$=0.7 and 300^0C, $CH_4/(CH_4+SiH_4)$=0.6) have the same bandgap, E_{tauc}=1.90eV and E_{04}=2.05 eV. The known sample on the graphs is a amorphous silicon sample which has Urbach energy of 50 meV, Tauc energy of 1.72 eV, and E_{04} energy of 1.82 eV. The sample that is grown at 350^0C has lightly higher fill factor because the Urbach energy is lower. The Urbach energy of 49 meV proves that the device quality is very good.

The fill factor of amorphous silicon carbide solar cells is strongly influenced by the thickness of the i-layer. The optimum thickness for the i-layer depends upon the localized state density. Light is absorbed more efficient if the i-layer is thicker, but conversely a weak electric field portion appears within the i-layer. This portion not only reduces the fill factor because of it series resistance, but it can also reduce the collection efficiency for the carriers excited near the i/n^+ interface. If the i-layer is thin, the fill factor increases due to the existence of a strong electric field across the entire i-layer region. However, short-circuit current decrease because light absorption falls. Figure 4.22 shows that the fill factor decreases significantly if the thickness of the i-layer is high. The current is higher if the i-layer is thicker.

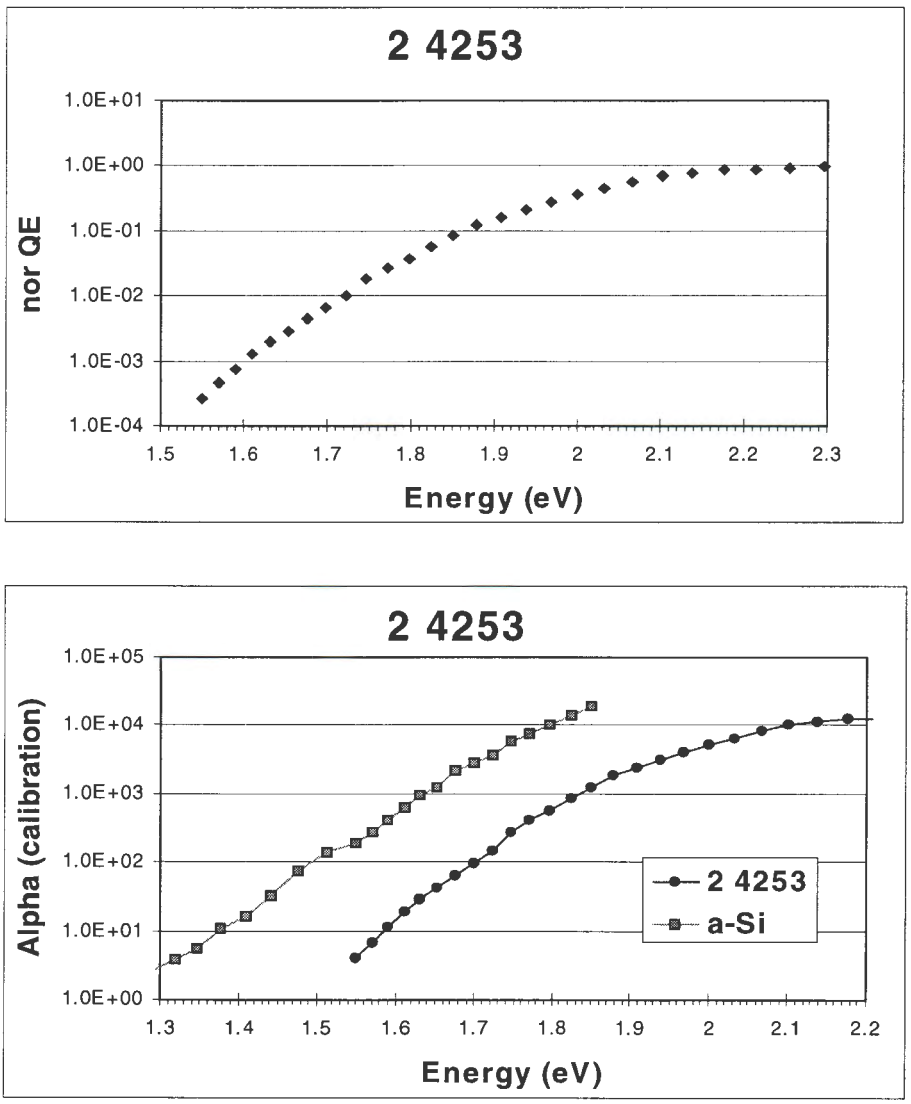

Figure 4.20: Urbach energy and bandgap of the 350^{0}C, $CH_4/(CH_4+SiH_4)=0.7$ device.

The diode quality factor of our devices is determined by the graph in Figure 4.23. Since the open-circuit voltage is related to the short-circuit current density by

$$\mathrm{Voc} = \frac{n'kT}{q}\left(\frac{\mathrm{Jsc}}{\mathrm{Jo}} + 1\right) \quad ,$$

The slope of the graph is 1/n'kT. Solve for n', we get 1.43 for the diode factor.

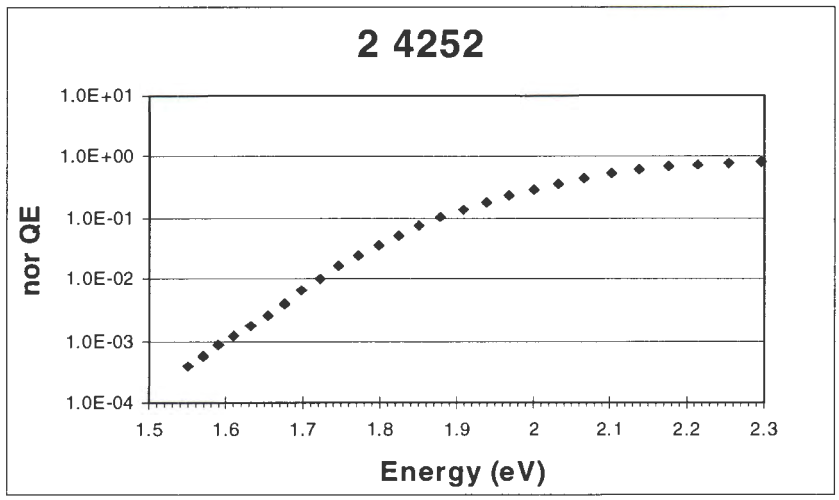

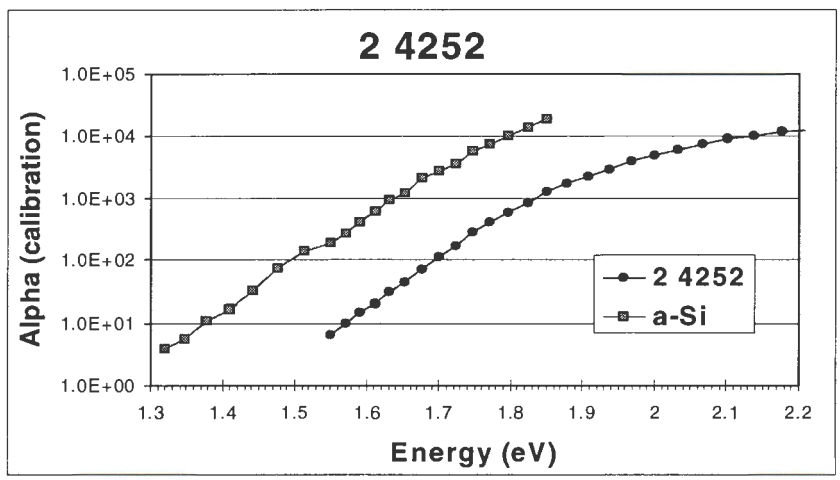

Figure 4.21: Urbach energy and bandgap of the 300^{0}C, $CH_4/(CH_4+SiH_4)$=0.6 device

The open-circuit voltage of our best sample is 0.91 V with chromium contacts. The semi-transparent metal contact of 10 nm thick chromium was measured to have about 25% transmission of visible light. Therefore, for 4 times greater flux

$$\Delta V_{oc} = 1.43\frac{kT}{q}\ln(4) \quad = .051V$$

So, if one sunlight get into the cells, the actual open-circuit voltage is 0.96 V.

In summary, we are able to produce the good devices. So far, we have devices that have E_{04} gap of 2.05eV, Urbach energy of 50 meV, open-circuit voltage of 0.94 to

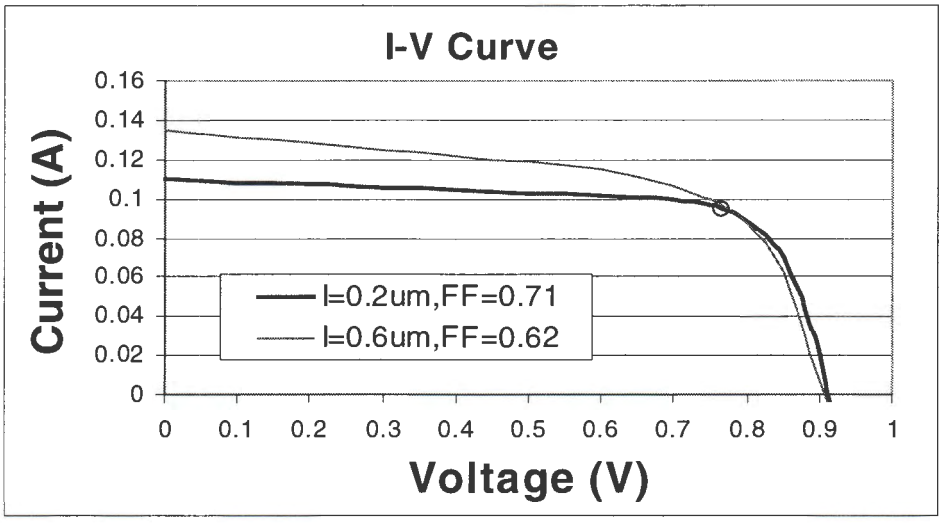

Figure 4.22: The thinner i-layer device has a higher fill factor. The two samples are grown in the same conditions and gas flow ratio. The only difference is the thickness

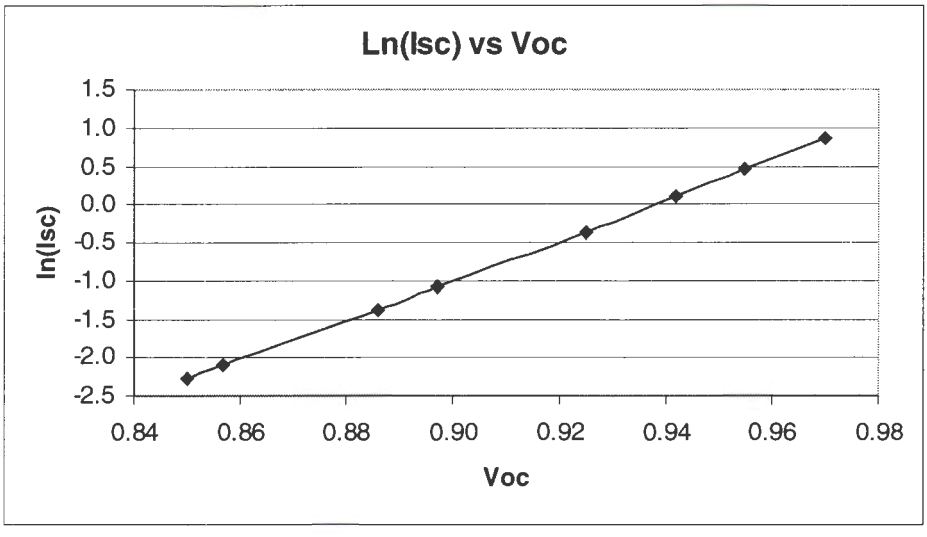

Figure 4.23: The measurement of diode quality factor

0.96 V, and fill factor up to 0.71. This shows that we can make good a-(SiC) solar cells using ECR technique. The open-circuit voltage of our amorphous silicon carbide solar cells is 0.1 V higher than it is for amorphous silicon solar cells. The fill factor of our amorphous silicon carbide solar cells is comparable to fill factor of amorphous silicon solar cells. They are 0.7 to 0.71.

CHAPTER 5: DISCUSSION

The device results that we have obtained are superior to the reported results of other groups working on amorphous silicon carbide solar cells. Swati Ray and Sukti Hazra of Indian Association for the Cultivation of Science got the open-circuit voltage of 0.925V for TCO coated glass (equivalent to 0.87V for chromium contacts), and the fill factor was 0.65 [12]. They used PECVD method to grow their samples at 200 to 250^{0}C. Wronski et al of Pennsylvania State University got the open-circuit voltage of 0.914V for TCO coated glass, and the fill factor was 0.61, and the stability was very low [16]. His p-i-n solar cells were grown at 200^{0}C, and the thickness of a-SiC:H i-layer was 0.2μm. Our samples had the same thickness, but they were grown at 300 and 350^{0}C, therefore the stability may be better.

We are able to produce good amorphous silicon carbide devices because our ECR deposition technique can produce good intrinsic and doped a-SiC:H materials. Figure 5.1 show that our intrinsic material has higher mobility-lifetime product compared to what have been reported in the literature[8]. Figure 5.2 shows that the Urbach energies on our films are also lower than other work. The Urbach energy of our devices and films are measured in both comparable at about 50 meV. In contrast, Y. M. Li of Solarex Corporation got the Urbach energy of 70 meV for the same bandgap [9].

We used amorphous silicon for the n-layer of most of the samples. N-layer is considered as a "dead" layer in the bottom of our solar cells, and so does not affect the properties of the solar cells. Its conductivity is high so that the resistivity of the solar cells is acceptable. The conductivity of our p-layer is compatible with that in the literature (Figure 5.3). It is in order of 10^{-6} $(\Omega cm)^{-1}$ for the bandgap of 2eV. The low deposition temperature yields the high bandgap and high enough conductivity p-layer.

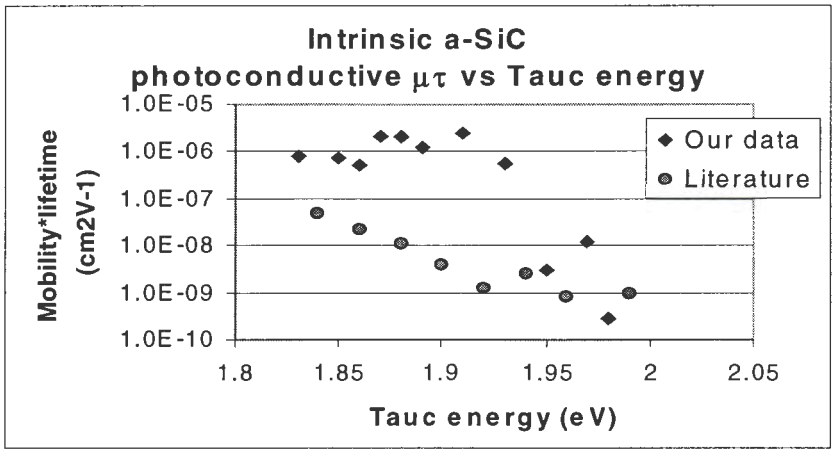

Figure 5.1: photoconductive versus optical bandgap.

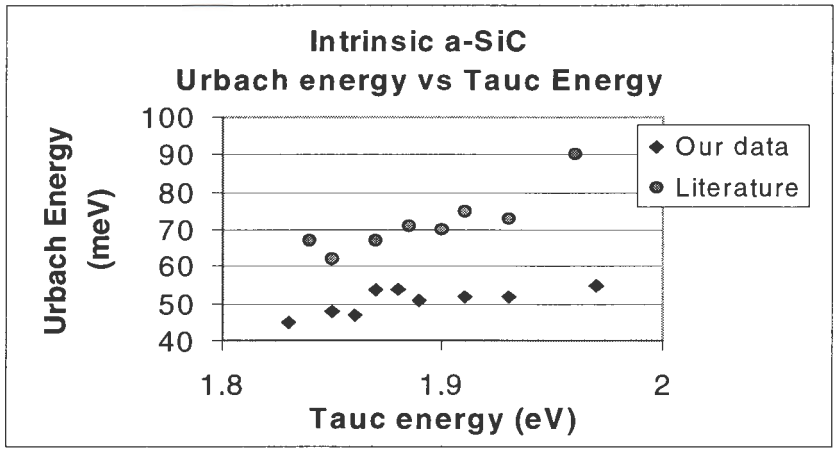

Figure 5.2: Urbach energy versus optical bandgap.

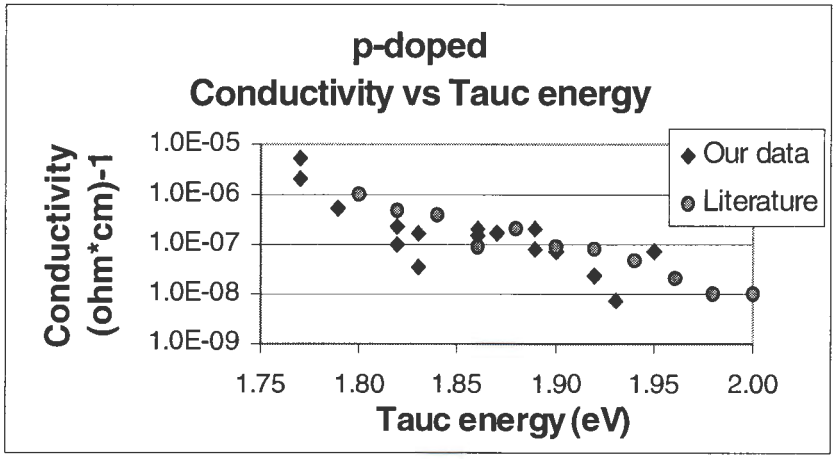

Figure 5.3: p-doped - photoconductivity versus optical bandgap.

CHAPTER 6: CONCLUSION

Amorphous silicon carbide has a large bandgap and good photosensitivity. It is an important material for potential application in photoelectronic devices, and is a promising material for the future development in the semiconductor and solar cells industries. Amorphous silicon carbide solar cells yield high quantum efficiency at low wavelengths, high open-circuit voltage and high fill factor as well.

We found the appropriate parameters to grow intrinsic amorphous silicon carbide film, which have good film quality, high electron mobility-lifetime products, low Urbach energy, high photosensitivity, and also have acceptable growth rate and expected bandgap, depending on the applications. The indicated substrate temperatures of 300 to 400^0C (real 250 to 350^0C) is a good range to deposit a-SiC:H by the ECR method. Hydrogen dilution is a better choice than Helium. The ratio of methane and silane flows can be varied to change the bandgap. Our intrinsic a-SiC:H materials have Urbach energy of around 50 meV for the optical bandgap in the range of 1.8 to 2.0 eV, and their mobility-lifetime product are in order of 10^{-6} cm^2/V. Our n-doped and p-doped a-SiC:H films have high conductivity. A substrate temperature of 200^0C was used to grow p-doped a-SiC.

We also used the remote ECR process to make p-i-n devices. We got good devices with open voltages up to 0.96 V, and fill factors up to 71% for a 0.2 μm i-layer thickness solar cell. The fill factor decreases if the thickness of the i-layer gets larger, because of the weaker electric field across the i-layer region. The i-layer of these solar cells are grown at 250 and 300^0C (real) with a doping of 10 per million diborane. The $CH_4/(CH_4+SiH_4)$ ratio is in the range of 0.6 to 0.7. Their optical bandgaps are 1.9 to 1.94 eV, and their Urbach energies are around 50 meV.

REFERENCES

[1] Brodsky M. H. Amorphous Semiconductors. Springer-Verlag Berlin, Heidelberg, 1979, pp. 123-128.

[2] Frantsevich I. N. Silicon Carbide. Consultants Bureau. New York, 1970.

[3] Gomez F. J. "Amorphous SiC Layers Deposited by ECR Plasma: Spectroscopic ellipsometric measurements". Journal of Non-crystalline Solids, 194, 1995, pp. 164-173.

[4] Hamakawa Y. "Physics and Application of Amorphous Silicon Carbide". Amorphous and Crystalline Silicon carbide and Related Material II. Springer-Verlag Berlin, Heidelberg 1989, pp. 164-168.

[5] Koji Akiyama. "Hydrogenated Amorphous Silicon Carbide Photoreceptor for Photoaddressed Spatial Light Modulator". Journal of Japanese Applied Physics. Vol. 32, 1993, pp. 590-599.

[6] Kuwano. "Amorphous Silicon Solar Cells Using a-SiC Materials". Amorphous and Crystalline Silicon Carbide. Springer Proceeding in Physics, Vol 34, pp. 167-177.

[7] Li Y. M. "Novel Feedstocks for a-SiC:H Films". Photovoltaic Specialist Conference. 1996 IEEE, pp. 229-237.

[8] Liu Chih-Chien. "Growth of SiC Film on Si(100) by Electron Cyclotron Resonance Chemical Vapor Deposition Using $SiH_4/CH_4/ H_2$". Electrochemical Soc., Vol 142, No.12, Dec. 1995, pp 2345-1249.

[9] Magalhaes Schmidt. "Photoluminescence Studies on Silicon Carbon Alloys". Journal of Non-crystalline Solids, 164-166, 1993, pp. 1027-1030.

[10] Masaki Shima. "Effect of Composition on the Properties of Amorphous Silicon Carbide at a Certain Optical Gap". Journal of Japanese Applied Physics. Vol. 36, 1997, pp. 2044-2048.

[11] Matsuda A. "Growth Mechanism of Hydrogenated Amorphous SIC from a Glow-Discharge Plasma". Amorphous and Crystalline Silicon Carbide. Springer Proceeding in Physics, Vol 56, pp. 45-51.

[12] Swati R. "Preparation of High and Low Bandgap Amorphous Silicon by PECVD and Their Application in Solar Cell". Photovoltaic Specialist Conference. 1996 IEEE, pp. 1077-1080.

[13] Takahashi K. Amorphous Silicon Solar Cells. North Oxford Academic Publishers, London, 1986

[14] Wang F. "Characterization of Optoelectronic Properties of a-$Si_{1-x}C_x$:H Films". Journal of Non-crystalline Solids, 164-166, 1993, pp. 1039-1042.

[15] Wronski C. R. "Wide Band Gap Solar Cells with High Stabilized Performance". Photovaltaics. US Department of Energy Annual Technical Report, 1997 CD Rom.

[16] Yoon S. F. "Some Effects of Boron Doping in a-SiC Films Prepared by the ECR-CVD Method". Journal of Non-crystalline Solids, 211, 1997, pp. 173-179.

[17] Yoon S. F. "Influence of Boron Doping on the Properties of Amorphous and Microcrystalline SiC Films Prepared Using ECR-CVD". Journal of Electronic Materials, Vol. 25, No. 12, 1996, pp. 1845-1850.

[18] Zedlitz R. "Amorphous Hydrogenated Silicon Carbon From VHF Deposition". Journal of Non-crystalline Solids, 164-166, 1993, pp. 1031-1034.

ACKNOWLEDGEMENTS

I would like to take this opportunity to thank the various people who have helped me to complete this research.

First and foremost, my sincere gratitude goes out to my major professor, Dr. Vikram Dalal for his valuable guidance and support throughout my research project. I am very appreciative that he gave me the opportunity to pursue certain aspects of the project. I also appreciate his financial support during my graduate years. I would also like to thank Dr. William Black and Dr. David Lynch for serving on my committee. I would also like to thank Tim Maxson, Kay Han, Jason Herrold, Bryan Oliver, and Matt DeFreese for providing me excellent training in ECR-CVD process, measurement taking, and academical helps. Thanks also go out to all members of Microelectronic Research Center for their friendship, guidance, support, and interesting discussions.

I would like to thank the Department of Electrical Engineering and Graduate College of Iowa State University for providing financial supports during the past two years of my works as a teaching assistant and research assistant at the Electrical Engineering Department and Microelectronic Research Center. I would like to thank Dr. Gary Tuttle and other faculty members of Electrical Engineering and Material Science Engineering for providing knowledgeable support during my educational experience.

Special thanks goes out to my former professor Ali Badakhshan of the University of Northern Iowa for research experiences and preparing me for graduate studies.

Finally, I would like to thank my parents, Mr. and Mrs. Minh Vu, and my wife, Thu Thuy, for their love and support during this research experience.